JCTC Journal of Chemical Theory and Computation

Perspective

Cite This: J. Chem. Theory Comput. 2019, 15, 1477−1491

pubs.acs.org/JCTC

Understanding Carrier Transport in Organic Semiconductors: Computation of Charge Mobility Considering Quantum Nuclear Tunneling and Delocalization Effects

Yuqian Jiang,[†] Hua Geng,[‡] Weitang Li,[§] and Zhigang Shuai*[,§]

[†]Laboratory for Nanosystem and Hierarchy Fabrication, CAS Center for Excellence in Nanoscience, National Center for Nanoscience and Technology, Beijing 100084, People's Republic of China

[‡]Department of Chemistry, Capital Normal University, Beijing 100048, People's Republic of China

[§]MOE Key Laboratory of Organic OptoElectronics and Molecular Engineering, Department of Chemistry, Tsinghua University, Beijing 100084, People's Republic of China

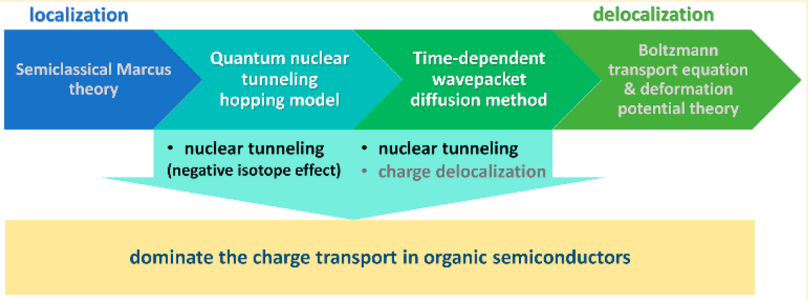

ABSTRACT: Despite great attention to the charge transport in organic semiconductors (OSC) over the last decades, the underlying mechanism is still controversial. After our theoretical position in 2009, the quantum nuclear tunneling effect has been proven by more and more experiments to play an essential role for charge transport in organic and polymeric materials. On the other hand, back in the 1970s, it was proposed that the nature of charge transport could be analyzed by the isotope effect, which, however, has not been confirmed either experimentally or theoretically. In this Perspective, we review the understanding of microscopic mechanisms on charge transport by using different transport mechanisms from hopping to band transport. Particularly, we point out that the isotope effect, which is absent in the semiclassical Marcus theory, should be negative for the localized charge transport with quantum nuclear tunneling. We conclude that the quantum nuclear tunneling effect dominates the charge transport in OSCs.

1. INTRODUCTION

Along with the improvement of fabrication methods and development of charge transport mechanisms for organic semiconductors in the last decades, numerous systems have been found to possess the room-temperature hole mobility as high as several tens of $cm^2\ V^{-1}\ s^{-1}$. Such high mobility existing in OSCs calls for a thorough understanding of charge transport mechanisms, for better designing molecules theoretically. However, the mechanism being hopping or bandlike transport is still controversial. The bandlike model with a fully delocalized picture has been used to describe the high mobility in OSCs, such as thienacene derivatives,[1−5] pentacene,[6] rubrene,[7−9] 6,13-bis(triisopropylsilylethynyl)pentacene (TIPS-P),[10] etc. However, compared with the experimentally measured carrier mobility, the bandlike model greatly overestimates the values of most systems,[11,12] and the typical temperature dependence does not always exist in high mobility systems, such as dinaphtho-thieno-thiophene (DNTT) single crystal transistor.[5] As a result, the reliability of the bandlike model applied in OSCs is questioned. For the materials with positively temperature-dependent mobility, the dominant transport mechanism was deemed to be thermally activated hopping. A fully localized hopping model dependent on the Marcus theory was proposed and achieved a great deal of success in designing materials.[13−17] The semiclassical Marcus theory[18] was originally developed to study the electron exchange reaction in solution by assuming that the electron was transferred after solvent reorganization, which was mainly associated with low-frequency polarization motion ($\omega \ll k_B T$). Thus, the environmental fluctuations were treated classically according to the high-temperature approximation, and the thermal activation vanishes at zero temperature. Nevertheless, in OSCs, both the intramolecular and intermolecular vibrations are coupled with the electronic degrees of freedom. Moreover, the typical vibration consists of conjugated C−C stretching, satisfying $\omega \gg k_B T$. Therefore, the classical treatment on environments in the Marcus theory should not be appropriate for OSC systems. In fact, a number of experiments observed finite conductivity in organic materials at very low temper-

Received: July 27, 2018
Published: January 8, 2019

DOI: 10.1021/acs.jctc.8b00779
J. Chem. Theory Comput. 2019, 15, 1477−1491

ature,[19−21] indicating that the quantum nuclear tunneling effect should be considered. In addition, the Marcus theory often underestimates the carrier mobility. For example, it predicted the hole mobility for pentacene as ca. 6−15 $cm^2 V^{-1} s^{-1}$,[22] while the recent experimental single crystal field-effect transistor (FET) mobility reached 15−40 $cm^2 V^{-1} s^{-1}$.[23] All the cases mentioned above pointed out the inadequacy of the Marcus theory in describing the charge transport mechanism and predicting mobility. To bridge the fully delocalized bandlike model and the fully localized Marcus theory, the quantum nuclear effect on charge transport was proposed.

Conducting polymers had been awarded the Nobel Prize in Chemistry in 2000, but the conducting mechanisms have been long elusive. Even the most recent theories are mutually exclusive, such as the 1D Luttinger liquid model,[19] the 3D environment Coulomb blockade model,[24] and the modified variable range hopping methods.[25] A recent proposed formula was based on the framework of quantum nuclear tunneling mechanism which could successfully fit the $J(V, T)$ curves for five different polymers,[21] helping to clarify the disputed transport mechanisms and revealing the universality of nuclear tunneling enabled polaron transport mechanism for conducting polymers. In fact, the quantum nuclear effect on charge transfer was earlier investigated by Ulstrup and Jortner,[26] and Emin had also looked at the polaron hopping effect long ago;[27] but for organic semiconductors, it was Nan et al., who first proposed an elaborated hopping model derived from Fermi's Golden rule which included a full quantum nuclear effect.[28] Quantum nuclear tunneling can effectively lower the barrier height, thereby enhancing the mobility. Such a quantum nuclear tunneling enabled hopping model naturally interpreted the paradoxical phenomenon observed in TIPS-P that the optical measurement indicated localized charge carriers, but the electrical measurement showed the bandlike temperature-dependent mobility.[29] More importantly, the quantum nuclear tunneling enabled localized charge transport has been proven by combined experimental and computational evidence by Taherinia et al.[30] and by van der Kaap et al.[31]

For the purpose of investigating the microscopic mechanism of charge transport, Munn et al. have put forward the proposal of studying the isotope effect on charge mobility as early as 1970 by using the Holstein model.[32] By assuming the quasi-localized electron and considering one or two oscillators, it was predicted that isotopic substitution could promote mobility in the "slow-electron" end and slower mobility in the "slow-phonon" end. Subsequently, the measurement of c' directional electron mobility in anthracene crystal exhibited an 11% increase upon all-deuteration, which seemingly matched the "slow-electron" mechanism.[33] In 1971, Morel and Hermann even observed a 3-fold increase in electron mobility in the c'-direction upon all-deuteration for anthracene.[34] Nevertheless, this result was soon overturned by them, and a 10% decrease in the c' directional mobility was published.[35] Later, an unnoticeable isotope effect on the electron mobility in the c' direction was measured in naphthalene by Schein and McGhie.[36] Similarly, Xie et al. recently observed an inappreciable isotope effect on hole mobility for all-deuterated rubrene.[9] Due to those mutually exclusive experiments and uncertain theoretical studies, there is still no definite answer as to whether or not the isotope effect exists.

On the other hand, extensive efforts on isotope effect have been carried out for understanding the nonradiative decay processes of molecular excited state[37−39] and the mechanisms of chemical reactions.[40−42] For instance, deuteration could greatly influence the nonradiative decay rate from the excited state (T_1 or S_1) to the ground state (S_0), and isotopic substitution occurring in the broken or formed bond could change the chemical reaction rate dramatically. These have been rationalized by the changes in frequency of phonon modes or chemical bonds after nuclear mass increasing. Thus, the isotope effect on charge transport should also be found in process where exists the optical phonon scattering from intramolecular vibrations, due to the lower nuclear vibrational frequency and weaker quantum nuclear effect upon heavier nuclei. Therefore, it is of great significance to give a systemic theoretical prediction on OSCs, especially by the quantum nuclear tunneling model.

It is noticed that either quantum nuclear tunneling or the Marcus theory describes a well localized charge transport picture, in which the intermolecular electronic transfer integral (V) is far less than the intramolecular reorganization energy (λ). As for the high mobility materials with comparable V and λ, it raises the question that whether the charge carrier is still localized in one molecule or delocalized in several neighbors. As a result, the intermediate regime situated between the localized and fully delocalized ends needs to be put forward. Electron quantum dynamics is such a good method which can study the degree to which the carrier wave function is extended over neighboring molecules and meanwhile be able to describe the coherent motion of the charge carrier. To include the influence of molecular vibrations on electrons, mixed quantum/classical dynamics (MQCD) approaches, such as surface hopping or Ehrenfest dynamics[43] and first-principles calculation based on the Su-Schrieffer-Heeger (SSH) type model,[44] have been widely proposed to study the charge transport property, especially for the real organic systems,[45,46] by treating nuclear motions classically. Full quantum dynamics (FQD) methods, like the nonperturbative hierarchically coupled equations of motion[47] and the non-Markovian stochastic Schrodinger equation,[48] have also been proposed for parametrized models rather than real organic materials, since the system sizes are limited to dozens of sites in the limitations of memory and numerical convergence. In order to overcome the computing restriction, Zhong et al. developed a more efficient FQD approach, namely time-dependent wavepacket diffusion (TDWPD), which includes the quantum nuclear effect by the harmonic oscillator model and is able to deal with even thousands of sites efficiently. Its benchmark work on charge transport[49] showed good consistency with the nonperturbative hierarchically coupled equations of motion as well as the path integral method, by which only small-sized symmetric systems could be studied. Moreover, it is proven that the TDWPD method is fairly effective on symmetric systems, although it is difficult to reproduce Boltzmann distribution in asymmetric systems.[50] Thus, for real homogeneous OSC systems, TDWPD is useful to discuss the electron delocalization and coherence as well as the quantum nuclear effects.

Our previous reviews summarized the progress in developing computational tools for mobility prediction starting from the Marcus theory,[17] and the evaluation of the quantum nuclear tunneling enabled the hopping model with several applications.[51] In this Perspective, we will focus on the recent progress in investigating the microscopic mechanisms of charge transport for OSCs by using the quantum nuclear tunneling model compared with the Marcus theory, the wavepacket

DOI: 10.1021/acs.jctc.8b00779
J. Chem. Theory Comput. 2019, 15, 1477−1491

diffusion approach, and the bandlike transport model. Namely, we are going to highlight the respective roles of quantum nuclear tunneling and charge delocalization played in charge transport.

2. ISOTOPE EFFECT ON CHARGE TRANSPORT

2.1. Isotope Effect in the Bandlike Limit with Acoustic Phonon Scatterings. As to which bandlike model is concerned, the electron coherent length is assumed to be far longer than the lattice spacing distance, and the electron de Broglie wavelength is about 7 nm at 300 K which matches the acoustic phonons. Thus, the electron−phonon coupling has been often evaluated by deformation potential through a lattice dilation/contraction scheme. Recently, Xi et al.[52] have applied a Wannier-interpolation technique including both acoustic and optical phonons scattering for computing the bandlike mobility of two-dimensional (2D) carbon materials. The acoustic phonons have been found to be dominant, while the optical phonons have little impact on scattering unless the temperature is high enough. Thus, the combination of the acoustic phonon based deformation potential (DP) theory and the Boltzmann transport equation[53] has been widely applied to study the bandlike transport behavior in OSCs.[11,54,55]

In order to investigate the isotope effect in bandlike transport, we take C_8-BTBT which is widely recognized as the band transport[1] to study the all-deuteration effect by the DP theory, the methodology of which is described in detail in ref 54. A refined introduction of the calculation method is presented here for better understanding of the calculation results. The Vienna ab initio simulation package (VASP 5.3.2)[56] is applied to optimize the geometries and calculate the band structures for pristine and all-deuterated C_8-BTBT. The cutoff energy for the plane-wave basis is set as 600 eV, and the cutoff radius for pair interactions is 50 Å. The spin−orbit coupling is not taken into account here. The Monkhorst−Pack **k**-mesh for calculating the ionic and lattice constant relaxations is 4 × 4 × 1 and for obtaining the single-point energy and charge density calculations is 8 × 8 × 2. The tetrahedron method with Blöch corrections is applied for smearing. The electrical conductivity σ in the Boltzmann transport theory[57,58] is determined by the transport distribution function $\sum_{\mathbf{k}} \mathbf{v}_{\mathbf{k}}\mathbf{v}_{\mathbf{k}}\tau_{\mathbf{k}}$, where $\boldsymbol{\tau}_{\mathbf{k}}$ is the relaxation time that measures how quickly the electrons restore the equilibrium distribution within phonon scattering. $\mathbf{v}_{\mathbf{k}} = \nabla_{\mathbf{k}}\varepsilon_{\mathbf{k}}/\hbar$ is the group velocity obtained by the band structure calculations, and $\boldsymbol{\varepsilon}_{\mathbf{k}}$ is the band energy at **k**-point. Here, a fine **k**-mesh of 41 × 41 × 9 is used for calculating the band energies for C_8-BTBTs. In the long wavelength limit, the scattering matrix element is assumed to be independent of the lattice wave propagation direction. Thus, the relaxation time can be expressed as $\frac{1}{\tau_k} = \frac{2\pi}{\hbar}|M(\mathbf{k}, \mathbf{k}')|^2 \sum_{k'} \delta(\varepsilon_k - \varepsilon_{k'})[1 - \cos\theta]$, where θ is the angle between **k** and **k**′, and $\delta(\varepsilon_{\mathbf{k}} - \varepsilon_{\mathbf{k}'})$ is Dirac delta function. The matrix elements for electrons scattered from Blöch state **k** to **k**′ is expressed as $|M(\mathbf{k}, \mathbf{k}')|^2 = k_B T E_1^2/C_{ii}$, where E_l and C_{ii} are the DP constant and the elastic constant, respectively, in the lattice wave propagation direction. For simplicity, we stretch the unit cell along *a* and *b* directions. With respect to the lattice dilation, E_l is calculated from a linear fitting of band edge energy shift values, while C_{ii} is obtained by parabolic fitting of the total energy values. After calculating the electrical conductivity through the Boltzmann transport theory, mobility can be finally achieved by $\sigma = Ne\mu$.

It is most interesting to note that our theoretical hole mobility for C_8-BTBT published in 2014 (165−180 $cm^2/(V\,s)$)[54] was confirmed two years later by the field-induced time-resolved microwave conductivity measurement by Tsutsui et al., who found a strikingly high room temperature average mobility of 170 $cm^2\ V^{-1}\ s^{-1}$ for 2,7-C_8-BTBT, strongly suggesting a bandlike behavior for BTBT due to the close molecular packing.[59] Second, it is noted that isotopic substitution leads to a slightly positive effect from Table 1.

Table 1. Deformation Potential Constants (E_l), Elastic Constants (C_{ii}), Relaxation Times (τ), and Mobility (μ) for Holes (h) and Electrons (e) in Pristine and All-Deuterated C_8-BTBTs along *a* and *b* Directions at Room Temperature[a]

	pristine	all-deuterated
$E_{l\,a}^{h}$ (eV)	1.39	1.39
$E_{l\,a}^{e}$ (eV)	2.29	2.29
$E_{l\,b}^{h}$ (eV)	2.73	2.73
$E_{l\,b}^{e}$ (eV)	0.74	0.74
C_{aa} (10^9 J/m^3)	18.3	18.3
C_{bb} (10^9 J/m^3)	9.91	9.76
τ^{h} (fs)	117	120
τ^{e} (fs)	50.3	51.3
μ_a^{h} ($cm^2/(V\,s)$)	180	184
μ_b^{h} ($cm^2/(V\,s)$)	165	171
μ_a^{e} ($cm^2/(V\,s)$)	13.4	13.6
μ_b^{e} ($cm^2/(V\,s)$)	28.1	28.8

[a]Table adapted with permission from Royal Society of Chemistry (ref 73).

This should be mainly ascribed to the tiny decrease on C_{bb} caused by a numerical error in the fitting process. Since both pristine and all-deuterated C_8-BTBTs share the same crystal structure, their electronic structures are identical to each other, and the group velocity will be unchanged. Accordingly, the band edge energy and the total energy with the same lattice dilation should also remain the same. Therefore, all-deuteration should have no effect on E_l and C_{ii}, and the relaxation times $\boldsymbol{\tau}_{\mathbf{k}}$ determined by $\mathbf{v}_{\mathbf{k}}$, E_l, and C_{ii} are supposed to be identical upon isotopic substitution. As a result, the electrical conductivities and the bandlike mobility should be independent of isotopic substitution, for both hole and electron transport.

2.2. Isotope Effect for Manifesting the Quantum Nuclear Tunneling in Hopping Transport. Based on the hopping mechanism, the charge transfer (CT) rate incorporating the quantum nuclear tunneling effect can be expressed as

$$k^{QM} = \frac{|V|^2}{\hbar^2}\int_{-\infty}^{\infty} \mathrm{d}t\ \exp\left\{it\omega_{fi} - \sum_j S_j[(2\bar{n}_j + 1) - \bar{n}_j e^{-i\omega_j t} - (\bar{n}_j + 1)e^{i\omega_j t}]\right\} \quad (1)$$

Here, ω_j and $\bar{n}_j = 1/[\exp(\hbar\omega_j/k_B T) - 1]$ are the frequency and the occupation number for the *j*-th vibrational mode, respectively, and S_j is the corresponding Huang−Rhys factor representing the local electron−phonon coupling. ω_{fi} is the site energy difference, which equals zero for monomolecular

DOI: 10.1021/acs.jctc.8b00779
J. Chem. Theory Comput. 2019, 15, 1477−1491

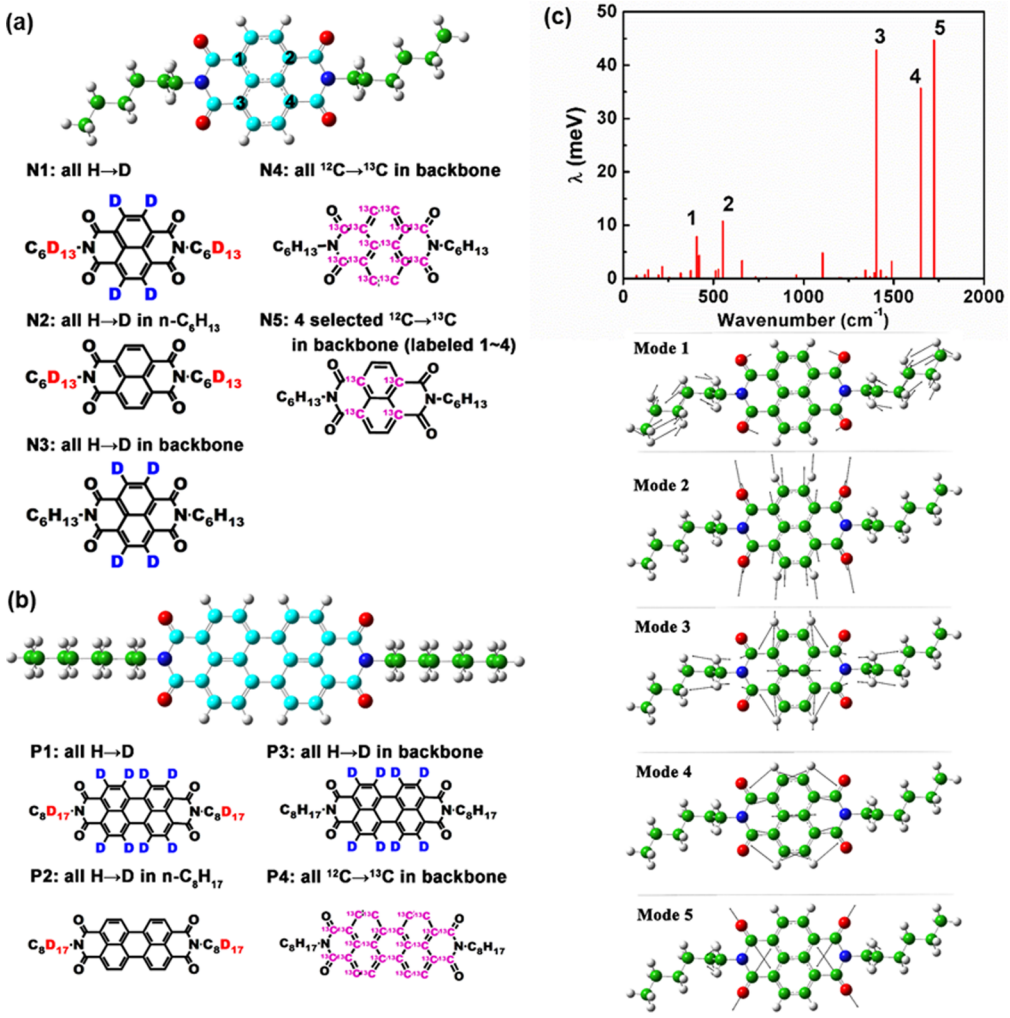

Figure 1. Schematic presentations of isotopically substituted (a) NDI-C6 and (b) PDI-C8. (c) The distribution of reorganization energies (λ) of all normal modes for pristine neutral NDI-C6 and the five modes with the largest reorganization energies are presented as well. Figure adapted with permission from American Chemical Society (ref 73).

crystals. In the limit of strong coupling where $\sum_j S_j \gg 1$, the short time approximation $\exp(i\omega t) = 1 + i\omega t + (i\omega t)^2/2$ can be applied. Meanwhile, in the case of high temperature approximation ($\hbar\omega_j/k_BT \ll 1$), the occupation number of phonons turns to $\overline{n}_j \approx k_BT/\hbar\omega_j$, thus eq 1 goes back to the Marcus formula

$$k^{SC} = \frac{|V|^2}{\hbar}\left(\frac{\pi}{\lambda k_B T}\right)^{1/2} \exp\left[-\frac{(\Delta G + \lambda)^2}{4\lambda k_B T}\right] \quad (2)$$

where the total charge reorganization energy is $\lambda = \sum_j \lambda_j = \sum_j S_j \hbar\omega_j$, and ΔG is the site energy difference. The carrier mobility is calculated via the Einstein formula $\mu = eD/k_BT$, where the diffusion coefficient D can be achieved by kinetic Monte Carlo simulation based on the CT rates. For the α-th pathway, the charge hops from molecule m to molecule n with the probability $p_\alpha = k^\alpha_{mn}/\sum_\alpha k^\alpha_{mn}$, and the simulation time is defined as $1/\sum_\alpha k^\alpha_{mn}$.[17,60] By averaging over thousands of trajectories, D can be finally calculated via $D = \lim_{t\to\infty} \frac{\langle R^2(t)\rangle}{2dt}$.

According to the Born−Oppenheimer approximation, the electronic structure determined properties, V and λ, are independent of isotope. Therefore, it is easy to find from eq 2 that the Marcus CT rate will not change after isotopic substitution. Thus, there should be no isotope effect found by using the Marcus theory. Comparatively, when the nuclear quantum effect is included as shown in eq 1, the CT rate will be sensitive to the isotope substitution by lowering the vibrational frequency and thus weakening the quantum effect. As a result, the charge transport will get close to the semiclassical end, and the CT rate as well as mobility are supposed to be lowered. Since there is almost no isotope effect in the bandlike mechanism, the observation of the negative isotope effect can directly manifest the quantum nuclear tunneling assisted hopping mechanism. In this section, we introduce our systematic theoretical predictions of the isotope effect on charge transport by the quantum nuclear tunneling model.

Among all isotopic substitutions, deuteration leads to the greatest increase in mass as 100%, while changing ^{12}C to ^{13}C only increases the mass by 8%. In OSCs, however, the conjugated C−C bond stretching vibrations play a significant role in phonon scattering. So both deuteration and ^{13}C substitution effects on charge transport have been investigated. As the typical n-type materials, we first take *N,N′*-bis(*n*-hexyl)naphthalene diimide (NDI-C6) and *N,N′*-bis(n-octyl)-perylene diimide (PDI-C8) as examples[61−64] to study their isotope effects by different isotopic substitutions, as shown in

DOI: 10.1021/acs.jctc.8b00779
J. Chem. Theory Comput. 2019, 15, 1477−1491

Figures 1a and 1b. All the optimizations and frequency analyses are calculated by the B3LYP functional combined with the 6-31G(d) basis set[65,66] by the Gaussian 09 package.[67] The calculation results show that the equilibrium geometry of each isotopic system is totally the same, while the frequencies decrease upon isotopic substitutions. Under the displaced harmonic oscillator approximation, the Huang−Rhys factor and reorganization energy of each mode are calculated through the normal-mode analysis method by the DUSHIN program.[68] The sum of all the normal mode reorganization energies is found to be almost identical to the total reorganization energy resulting from the adiabatic potential method, the values of which are 351 (350) meV for NDI-C6 and 272 (271) meV for PDI-C8, respectively. Moreover, the total reorganization energies obtained from the two methods are found to be independent of isotopic substitutions. By assuming the same crystal structures[62,63,69] for different isotopes, the transfer integrals obtained at the PW91PW91/6-31G(d)[70] level with the site-energy corrected coupling method[71] are indeed independent of isotope. The largest V in NDI-C6 and PDI-C8 is 74 and 44 meV, respectively, making both systems satisfy the condition of the hopping mechanism as $V \ll \lambda$. All CT rates and mobility calculations are performed by the home-made MOMAP program package.[72]

It should be noticed that, as for the quantum CT rate in eq 1, the time integration part being of oscillation behavior can reach the convergence only when the Huang−Rhys factor is large enough. For example, for rubrene, the numerical integration is convergent due to the large Huang−Rhys factor contributed by phenyl twisting motions,[28] while for NDI-C6 or PDI-C8, no mode can provide the convergence condition. Thus, the Lorentzian factor $e^{-\Gamma|t|}$ has been added for both NDI-C6 and PDI-C8, and the broadening Γ is set as small as 10 cm^{-1}, being treated as the environmental dissipation.

The electron mobility resulting from the Marcus theory is 0.24 $cm^2\ V^{-1}\ s^{-1}$ for all six isotopically substituted NDI-C6 and 0.50 $cm^2\ V^{-1}\ s^{-1}$ for the five isotopically substituted PDI-C8, indicating no isotope effect existed in the semiclassical limit. In addition, the Marcus theory underestimates the mobility values for both NCI-C6 and PDI-C8. The quantum nuclear tunneling model makes more reasonable prediction on mobility values compared to experiments[74,75] (Table 2) and indicates negative isotope effects for all the substitutions. For example, for either system, all-deuteration (**N1**, **P1**) and alkyl chain deuteration (**N2**, **P2**) lead to the strongest isotope effects, all of which reduce mobility more than 10%. All ^{13}C-substitutions on backbone also show obvious isotope effects such as −7% and −10% for **N4** and **P4**, respectively. To the contrary, no noticeable isotope effect has been found in other systems (**N3**, **P3**, and **N5**). The isotope effect derived from the quantum nuclear tunneling model has been rationalized by analyzing the electron−phonon couplings of normal modes. Modes with a large Huang−Rhys factor possess strong scattering ability. When the isotopic substitution happens on the atoms with major contribution to the vibrations of such modes, the corresponding frequencies would decrease remarkably. Then, the phonon scattering will be obviously enhanced and the nuclear tunneling will be greatly weakened in the case of keeping the total reorganization energy unchanged, thus resulting in a strong negative isotope effect on the CT rate or mobility. To explain this, the five dominated normal modes with the largest reorganization energies and corresponding frequencies for all NDI-C6 systems have been presented in Figure 1c and Table 3, where Mode 1 primarily consists of the rocking vibration of alkyl chains and Modes 2−5 involve in-plane bending of aromatic rings, conjugated C−C stretching, and C═O stretching vibrations, respectively. Among the systems with a strong isotope effect, all-deuteration on alkyl chains (**N1**, **N2**) leads to a remarkable frequency decrease on Mode 1, while all ^{13}C-substitution on backbone (**N4**) causes significant reductions in the frequencies of Modes 2−5. To the contrary, little frequency change of the five modes has been found in **N3** and **N5**, both of which exhibit weak isotope effects.

We then extend our study on the p-type material rubrene to compare with the recent experiment that all-deuterated rubrene shows no appreciable isotope effect.[9] It is noted that rubrene has been proposed to be best described by the bandlike model,[7] and comparable values between V and λ are actually found in both pristine and all-deuterated rubrenes, where λ is calculated as 150 meV, and the largest V is 83 meV. However, experimental research on tetracene, the parent of rubrene, revealed that it was the hopping mechanism dominating the transport process,[76] indicating the applicability of the quantum nuclear tunneling model on tetracene and

Table 2. Theoretical Electron Mobilities (μ_e, $cm^2\ V^{-1}\ s^{-1}$) and Corresponding Isotope Effects (IE, %) Defined as $(\mu_{Ni}-\mu_{N0})/\mu_{N0}$ in the Quantum Nuclear Tunneling Model for All NDI-C6 and PDI-C8 Systems at Room Temperature[c]

NDI-C6	μ_e	IE	PDI-C8	μ_e	IE
N0	4.31	0.00	P0	13.19	0.00
N1	3.44	−20.18	P1	11.11	−15.77
N2	3.55	−17.63	P2	11.53	−12.58
N3	4.27	−0.93	P3	12.89	−2.27
N4	4.02	−6.73	P4	11.87	−10.01
N5	4.28	−0.70			
Marcus	0.24		Marcus	0.50	
exp.	0.7[a]		exp.	1.7[b]	

[a]Reference 63. [b]Reference 65. [c]The isotope-independent Marcus electron mobilities and nonisotopically substituted experimental data are comparably given. Table adapted with permission from American Chemical Society (ref 73).

Table 3. Frequencies (cm^{-1}) of the Five Normal Modes for All Isotopic NDI-C6 Systems As Shown in Figure 1c[a]

	mode frequencies				
	1	2	3	4	5
N0	405.41	557.00	1450.90	1646.63	1781.34
N1	391.65	551.47	1446.22	1632.79	1779.00
	(3.39%)	(0.99%)	(0.32%)	(0.84%)	(0.13%)
N2	392.17	556.55	1450.37	1646.62	1779.16
	(3.26%)	(0.08%)	(0.04%)	(0.00%)	(0.12%)
N3	404.39	552.99	1446.24	1632.82	1781.18
	(0.25%)	(0.72%)	(0.32%)	(0.83%)	(0.01%)
N4	404.77	546.09	1394.99	1585.83	1735.63
	(0.16%)	(1.96%)	(3.85%)	(3.69%)	(2.57%)
N5	405.14	554.78	1424.78	1632.27	1780.51
	(0.07%)	(0.40%)	(1.80%)	(0.87%)	(0.05%)

[a]The relative frequency reductions of **N1**−**N5** compared to **N0** are provided in parentheses. Table adapted with permission from American Chemical Society (ref 73).

DOI: 10.1021/acs.jctc.8b00779
J. Chem. Theory Comput. 2019, 15, 1477−1491

Table 4. Isotope Effects (IE, %) on the CT Rate Defined as $(k_{iso}-k_0)/k_0$ after All ^{13}C-Substitution (^{12}C → ^{13}C) and All-Deuteration (H → D) for Four Acenes and Five Acene Derivatives[a]

		hole				electron			
		^{12}C→^{13}C IE	H→D IE	λ_{NM}	λ_{AP}	^{12}C→^{13}C IE	H→D IE	λ_{NM}	λ_{AP}
acenes	2A	−4.55	−0.86	189	187	−8.81	−6.41	262	261
	3A	−3.12	−0.33	141	139	−8.22	−5.33	198	198
	4A	−2.80	−0.47	120	116	−7.76	−4.88	164	162
	5A	−2.66	−1.05	94	94	−7.42	−4.37	132	132
derivatives	**1**	−9.75	−6.46	160	158	−10.56	−10.60	199	197
	2	−7.84	−4.35	141	140	−8.05	−4.45	184	183
	3	−3.09	−0.28	139	138	−7.63	−4.90	174	174
	4	−8.61	−5.19	159	167	−9.59	−5.96	176	174
	5	−7.03	−14.76	137	134	−9.59	−16.11	199	197

[a]The corresponding total reorganization energies (λ, meV) calculated by normal mode analysis (NM) and the adiabatic potential method (AP) are also given. Table adapted with permission from Royal Society of Chemistry (ref 77).

possibly its derivatives as well. The hole mobilities of pristine and all-deuterated rubrene calculated by the quantum nuclear tunneling model are 17.12 cm^2 V^{-1} s^{-1} and 16.68 cm^2 V^{-1} s^{-1}, which agree well with their experimental mobilities that both values are ca. 15 cm^2 V^{-1} s^{-1}. The slight isotope effect of all-deuterated rubrene is ascribed to the fact that aromatic hydrogen atoms make little contribution to the vibrations with major charge reorganization, which is similar to the situation in backbone deuterated NDI-C6 and PDI-C8 (**N3**, **P3**). Thus, the measurement of the deuteration effect could not help to distinguish the transport mechanism for rubrene. To figure out the significance of the nuclear tunneling effect and the dominance of hopping or bandlike transport, it is necessary to study the isotopic systems that substituted atoms involve actively in the vibrations with major contribution to charge reorganization. If the noticeable isotope effect can be observed in such isotopic substitutions, the quantum nuclear tunneling effect within a hopping model will be manifested.

2.3. Negative Isotope Effect for Charge Transport in Acenes and Derivatives. As introduced above, even though the isotope effect was earlier proposed to determine the charge transport mechanism in acenes, there still has been no definitive answer as to whether such an isotope effect is positive or negative for nearly half a century, since either the experimental measurement or theory was too rough to make a judgment. Therefore, in order to give a certain conclusion, we have systematically studied the isotope effect on both electron and hole transport for acenes and their derivatives by the quantum nuclear tunneling model. Since isotopic substitution is assumed to have no influence on the crystal structure and the intermolecular transfer integral, for simplicity, we here calculate the isotope effect on the CT rate instead of mobility. We first study the influence of all-deuteration and all ^{13}C-substitution on naphthalene (2A), anthracene (3A), tetracene (4A), and pentacene (5A) for both hole and electron transport, and our calculations show that all-deuteration or all ^{13}C-substitution could reduce both hole and electron transfer rates, as shown in Table 4. The results are consistent with our previous theoretical study, further validating the negative isotope effect on charge transport accompanying the quantum nuclear tunneling effect. The theoretical deuteration effect on anthracene mismatches with the experimental result in ref 32 but shows good consistency with Morel's measurement on the *c* direction's electron mobility for all-deuterated anthracene,[35] implying the existence of the quantum nuclear tunneling effect in anthracene. It needs to mention that, except in the *c* direction, neither in the *a* nor in the *b* direction had the isotope effect been observed.[35] This might be ascribed to the bandlike mechanism dominated by acoustic phonon scattering as introduced in section 2.1.

In Table 4, all-deuteration leads to slight isotope effects on hole transport for four acenes but more noticeable (ca. 5%) for electron transport. All ^{13}C-substitution leads to stronger isotope effects on both hole and electron transports, and the isotope effects on electron transport (ca. 7−9%) are about double the effects on hole transport (ca. 3−5%). Moreover, except for the negligible deuteration effect on hole transport, other isotope effects show decreasing trends with longer conjugation length and smaller total reorganization energy (Table 4). According to the previous study, the necessity for obtaining strong isotope effects is substituting the atoms with active participation in the vibrational modes which make significant contribution to charge reorganization. For acenes, the vibrational modes which contribute most to the reorganization energy are aromatic C−C stretching vibrations. Therefore, we can define an effective mode expressed as[78]

$$\omega_{eff} = \sqrt{\sum_i \omega_i^2 \lambda_i / \sum_i \lambda_i} \tag{3}$$

For hole transport in acenes, all the effective frequencies fall in the range of 1400−1500 cm^{-1} (Table 5). All-deuteration on four acenes leads to slight reduction on the effective frequency, so that the corresponding isotope effects are negligible. To the contrary, ^{13}C-substitution causes ca. 3.6% reduction on the effective frequency for all acenes, so that the ^{13}C-subsituted effect is remarkably increased. For electron transport in acenes, the effective frequencies are in the range of 1100−1300 cm^{-1}. For either hole or electron transport, ^{13}C-substitution leads to a larger frequency reduction than all-deuteration, leading to a stronger isotope effect than deuteration. Moreover, with the similar effective frequency decreases upon ^{13}C-substitution for all acenes, the larger electron reorganization energy will cause more increase in the Huang−Rhys factor compared to the hole transport process, leading to a stronger ^{13}C-substitution effect on electron transport than hole transport. In addition, much more frequency reduction upon all-deuteration during the electron transport process can lead to a much stronger isotope effect than the hole transport process.

We then extended our investigations to acene derivatives, bis(phenylvinyl)anthracene (**1**), bis(phenylethynyl)anthracene (**2**), dichlorotetracene (**3**), tetrachlorotetracene (**4**), and TIPS-

DOI: 10.1021/acs.jctc.8b00779
J. Chem. Theory Comput. 2019, 15, 1477−1491

Table 5. Effective Frequencies (cm^{-1}) of Pristine, All ^{13}C-Substituted, and All-Deuterated Acenes for Hole and Electron Transport[a]

	2A			3A			4A			5A		
	$C_{10}H_8$	$^{13}C_{10}H_8$	$C_{10}D_8$	$C_{14}H_{10}$	$^{13}C_{14}H_{10}$	$C_{14}D_{10}$	$C_{18}H_{12}$	$^{13}C_{18}H_{12}$	$C_{18}D_{12}$	$C_{22}H_{14}$	$^{13}C_{22}H_{14}$	$C_{22}D_{14}$
hole	1512.88	1453.99	1509.07	1521.02	1461.98	1515.85	1488.71	1430.91	1483.68	1452.36	1396.16	1446.55
		(−3.89%)	(−0.25%)		(−3.88%)	(−0.34%)		(−3.88%)	(−0.34%)		(−3.87%)	(−0.40%)
electron	1336.05	1288.16	1306.54	1263.93	1218.55	1236.47	1218.58	1174.63	1193.56	1182.47	1139.77	1158.246
		(−3.58%)	(−2.21%)		(−3.59%)	(−2.17%)		(−3.61%)	(−2.05%)		(−3.61%)	(−2.05%)

[a]The relative frequency changes upon all ^{13}C-substitution and all-deuteration are presented in parentheses. Table adapted with permission from Royal Society of Chemistry (ref 77).

P (**5**), as shown in Figure 2. The all ^{13}C-substitution and all-deuteration effects on hole and electron transport have also been calculated (Table 4). By introducing the side chains with dramatic influence on the reorganization energy distribution of acenes, such as phenyl (**1**, **2**), chlorine (**4**), and alkyl (**5**), stronger isotope effects on both electron and hole transport can be achieved, since the contribution to electron−phonon coupling made by side chains gets increased. Thus, isotopic substitutions on side chains can lead to remarkable enhancements of the Huang−Rhys factor compared to acenes, then resulting in great increases on the isotope effect. For instance, all ^{13}C-substitution effects on hole transport get increased 2−3 times after introducing the side chains into acenes as derivatives **1**, **2**, **4**, and **5**, and all-deuteration effects on hole transport are even 1 order of magnitude increased after side-chain substituting acenes. Especially for TIPS-P, all-deuteration leads to ca. 15% reductions in both hole and electron transport.

3. NUCLEAR TUNNELING AND CARRIER DELOCALIZATION: BRIDGE THE GAP BETWEEN HOPPING AND BANDLIKE TRANSPORT

To further reveal the significance of the quantum nuclear effect and evaluating carrier mobility, especially in high mobility OSC systems, we provided a comprehensive computational tool to study the charge transport property by employing four different methods covered from the semiclassical Marcus theory, to the quantum nuclear tunneling model, to quantum wavepacket diffusion, and eventually to the bandlike description under the DP approximation. The transport mechanism in real systems should always belong to one of them.

We will first give a brief introduction of the TDWPD method. The Hamiltonian for a carrier motion process can be expressed as

$$H(t) = \sum_{i=1}^{N} (\varepsilon_{ii} + F_i(t))|i\rangle\langle i| + \sum_{i\neq j}^{N} (\varepsilon_{ij} + V_{ij}(t))|i\rangle\langle j| \quad (4)$$

where $|i\rangle$ represents the electronic state of the i-th site, and $F_i(t)$ and $V_{ij}(t)$ are the fluctuations of site energy ε_{ii} and transfer integral ε_{ij} separately. The spectral density function of electron−phonon interaction $J(\omega) = \frac{\pi}{2}\sum_j \frac{\chi_j^2}{\omega_j}\delta(\omega - \omega_j)$ is employed for obtaining the memory effect of site energy fluctuation. Here, the electron−phonon interaction strength of the j-th normal mode is defined as $\chi_j = \Delta Q_j \omega_j^2$, where ΔQ_j and ω_j are the displacement and frequency of the j-th mode. The δ-function in spectra density is evaluated with Lorentz distribution $\delta(\omega - \omega_j) = \frac{1}{\pi}\frac{a}{a^2 + (\omega - \omega_j)^2}$. Based on $J(\omega)$, a modified spectral density function at a certain temperature T which satisfies the detailed balance condition can be obtained as $G(\omega) = J(\omega)\ \coth\ (\beta^T\omega/2)/\pi$, where $\beta = 1/k_BT$. Subsequently, the site energy fluctuation will be calculated through $F_i(t) = \sum_{n=1}^{N}[2G(\omega_n)\Delta\omega]^{1/2}\cos(\omega_n t + \phi_n)$. By setting the upper cutoff frequency as ω_{max}, $\Delta\omega = \omega_{max}/N$, and $\omega_n = n\Delta\omega$. ϕ_n is the independent random phase which is uniformly distributed in the range of $[0, 2\pi]$.

For describing electronic dynamics, the Chebyshev polynomial expansion method is used to solve the time-dependent Schrödinger equation.[79] Once the wave function $\psi(t) = \sum_i^N c_i(t)|i\rangle$ is obtained, the diffusion coefficient D

DOI: 10.1021/acs.jctc.8b00779
J. Chem. Theory Comput. 2019, 15, 1477−1491

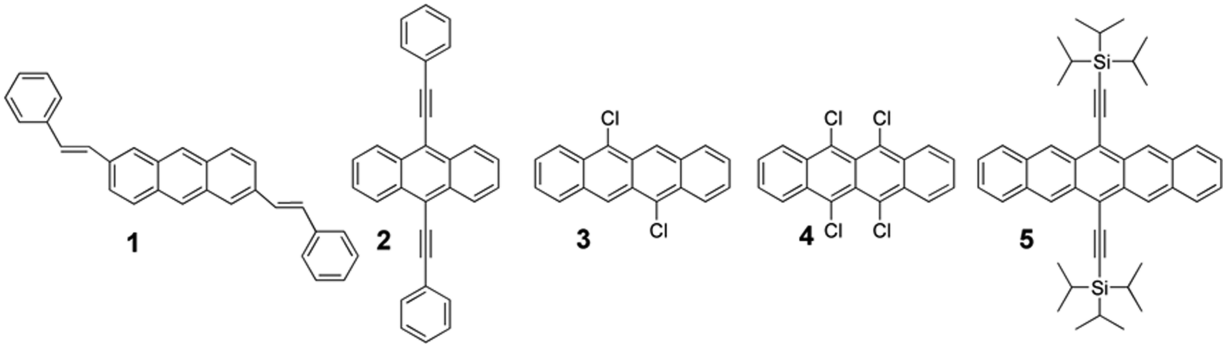

Figure 2. Molecular structures of the common acene derivatives considered. Figure adapted with permission from Royal Society of Chemistry (ref 77).

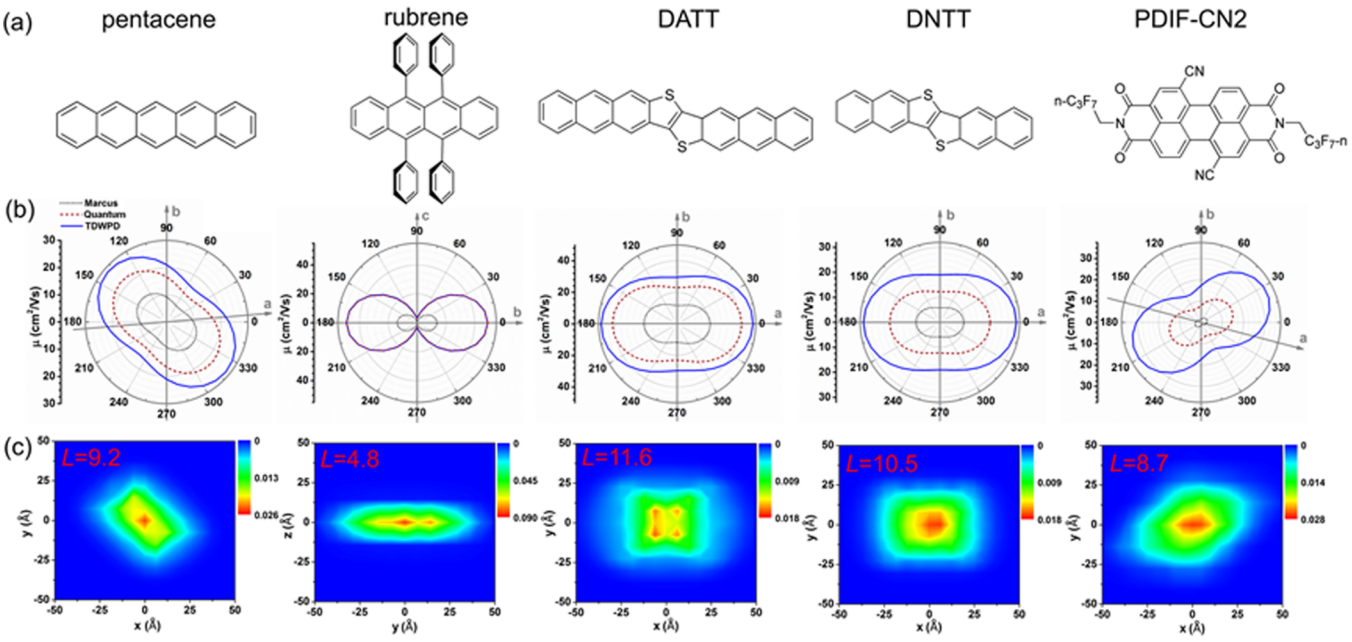

Figure 3. (a) The molecular structures of the five investigated OSCs; (b) the anisotropic mobilities resulting from Marcus, quantum nuclear tunneling, and TDWPD methods; (c) the distributions of charge population at 1000 au obtained from the TDWPD method, and the corresponding 2D electronic delocalization lengths (L) are given. Figure adapted with permission from Royal Society of Chemistry (ref 84).

can result from $D = \lim_{t\to\infty} \frac{\langle R^2(t)\rangle}{2dt}$. Here, d is the space dimension, and $\langle R^2(t)\rangle = \sum_i^N r_i^2 \rho_{ii}(t)$ where $\rho_{ii}(t) = \langle c_i^*(t)\, c_i(t)\rangle$ is the charge population of site i at time t, and r_i is the distance from site i to site a. When $t = 0$, one charge is set to be fully localized on site a, and $\langle R^2(0)\rangle = 0$. $\langle R^2(t)\rangle$ will become linearly increased with time after a certain time by averaging over hundreds of independent trajectories.

We have made a detailed and comprehensive investigation on several OSCs with high mobility, where pentacene, rubrene, dinaphtho-thieno-thiophene (DNTT), and dianthra-thieno-thiophene (DATT) are typical p-type materials, while PDIF-CN2 is n-type (Figure 3a). The mobility values obtained from all the methods are listed in Table 6. We only calculate the transport in the 2D plane because the interlayer coupling is extremely weak, and then we make spatial average for three-dimension. The optimization of neutral and charge geometries and corresponding frequency analyses are also performed by the B3LYP/6-31G(d) method. In TDWPD calculations, the models used for simulations for all systems are 41 × 41 clusters. The transfer integral fluctuation induced by lattice vibrations is not included, since several theoretical works indicated that the lattice dynamic disorder had little influence on the 2D transport property for OSCs.[50,80,81] As the angular-dependent mobilities show in Figure 3b, Marcus, quantum nuclear tunneling, and TDWPD approaches result in similar anisotropic behavior, simply because all of the three methods are random walk based. Among all the systems, rubrene possesses the strongest anisotropic transport property, while DNTT has the weakest anisotropy. Both of them show good agreement with experiments,[5,82,83] indicating the reliability of random walk simulation.

When compared to experiments, the DP theory is found to remarkably overestimate the mobility for all systems. Especially for rubrene, DATT, DNTT, and PDIF-CN2, their mobilities are at least 1 order of magnitude overvalued. Therefore, the rationality of bandlike transport mechanism in describing the organic systems should be questioned. As we have explained,[29] the so-called bandlike temperature behavior can be interpreted by a nuclear tunneling enabled localized picture instead. Besides, the semiclassical Marcus theory excluding the quantum effect can underestimate all the mobilities. Only the

DOI: 10.1021/acs.jctc.8b00779
J. Chem. Theory Comput. 2019, 15, 1477−1491

Table 6. Theoretical Mobilities ($cm^2 V^{-1} s^{-1}$) along *a*, *b*, and *c* Directions and the 3D-Averaged (AVG) Mobility Resulting from Marcus, Quantum Nuclear Tunneling, and TDWPD, as well as DP Methods[h]

	Marcus	quantum	TDWPD	DP	exp.
pentacene	*a*: 9.4	*a*: 16.9	*a*: 21.8	*a*: 58.0	15−40[a]
	b: 9.3	*b*: 16.7	*b*: 21.1	*b*: 44.0[b]	
	AVG: 6.7	AVG: 11.8	AVG: 15.1		
rubrene	*b*: 13.8	*b*: 48.9	*b*: 49.0	*b*: 242.6	15−17[c]
	c: 0.8	*c*: 2.8	*c*: 3.2	*c*: 72.7	
	AVG: 4.9	AVG: 17.2	AVG: 17.4		
DATT	*a*: 21.2	*a*: 41.3	*a*: 48.3	*a*: 322.6	16[d]
	b: 11.6	*b*: 23.0	*b*: 29.6	*b*: 19.1[e]	
	AVG: 10.6	AVG: 21.1	AVG: 25.2		
DNTT	*a*: 9.5	*a*: 20.2	*a*: 30.7	*a*: 137.7	6.8−7.5[f]
	b: 5.8	*b*: 12.2	*b*: 19.0	*b*: 76.4[e]	
	AVG: 5.1	AVG: 10.7	AVG: 16.3		
PDIF-CN2	*a*: 2.3	*a*: 12.1	*a*: 25.9	*a*: 132.8	1−6[g]
	b: 1.5	*b*: 8.0	*b*: 17.4	*b*: 91.2	
	AVG: 1.4	AVG: 7.5	AVG: 16.1		

[a]Reference 6. [b]Reference 12. [c]Reference 9. [d]Reference 16. [e]Reference 11. [f]Reference 5. [g]Reference 85. [h]The experimental values are also given for comparison. Table adapted with permission from Royal Society of Chemistry (ref 84).

quantum nuclear tunneling hopping model and the TDWPD approach can give reasonable results, again clarifying the importance of the nuclear tunneling effect on charge transport.

Different than the quantum nuclear tunneling model, the TDWPD approach additionally includes the electronic delocalization with coherence effect, which can facilitate charge transport. Therefore, in principle, it can lead to a larger mobility value than the quantum nuclear tunneling model, as seen in Table 6. In order to simplify the calculation of the correlation function, we only take the real part of fluctuation into account here. Actually, it has been proven that the particle dynamics induced by ignoring the imaginary fluctuation is small.[49] To qualitatively understand the coherent motion of charge carrier, the time-dependent charge populations of the initial site *a* have been plotted in Figure 4. For all systems, the oscillations of charge population have been observed during the decay process within 1000 au, illustrating the coherent carrier motion. Nevertheless, the oscillating behaviors disappear, and the quasi-thermal equilibriums of diffusions are achieved after 1000 au, indicating the loss of electronic coherence. The same phenomenon has also been found in pentacenequinone derivatives which has been rationalized by the fact that the electronic coherence between two adjacent sites could be broken down by nuclear tunneling resulting from high frequency vibrations.[50] Thus, we take the view that it is the electronic delocalization effect resulting in larger mobility values in the TDWPD mechanism.

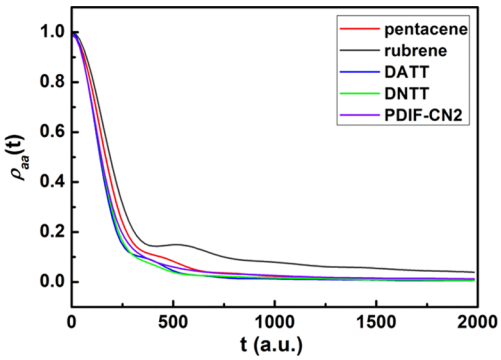

Figure 4. Time-dependent charge population on initial site *a* ($\rho_{aa}(t)$) for all systems in TDWPD simulations. Figure adapted with permission from Royal Society of Chemistry (ref 84).

The electronic delocalizations at 1000 au obtained by TDWPD are presented in Figure 3c for all systems, and the delocalization length is calculated by $L = \sqrt{1/\sum_{i=1} |c_i|^4}$. It is observed that the delocalization length of rubrene is shortest, which is only half of the delocalization length in DNTT or PDIF-CN2, although the experimental mobility of rubrene is much larger. This can be attributed to the strong anisotropic transport property of rubrene crystal that the 1D-like charge transport can lead to the weaker delocalization effect. Hence, the TDWPD method results in a similar mobility as the quantum nuclear tunneling model for rubrene. To the contrary, the charge delocalization effect seems to be very important in the other four systems, so that TDWPD results in a noticeable increase in their mobility compared to the quantum nuclear tunneling model. Therefore, we demonstrate that the simple nuclear tunneling enabled hopping model should be adequate if the charge delocalization effect is weak, like in rubrene. When the systems possess a relatively strong delocalization effect, such as pentacene, DATT, DNTT, and PDIF-CN2, the wavepacket description including a nuclear tunneling effect should be more preferred.

4. APPLICATION OF THE QUANTUM NUCLEAR TUNNELING MODEL TO A MOLECULAR BLENDING EFFECT ON CHARGE TRANSPORT

Molecular doping is a popular and efficient tool to improve the performance of organic electronic devices and control the carrier mobility in OSCs. Schwarze et al. reported that the band structures in OSCs could be modulated by blending organic small molecules,[86] providing a new aspect for material design. Both trapping and scattering effects[87−90] for doped disordered organic semiconductors have been studied based on the Gaussian disorder model (GDM).[91] Such an approach can indeed fit very well the device performances using a number of parameters, but it has less to do with molecular design. On the other hand, first-principle based methods starting from an ordered structure with well-defined molecular parameters are relevant to understand the structure−property at the molecular level. So we take crystalline structure as a prototype to understand the doping effect at the first-principle level with the quantum nuclear tunneling model.

TIPS-P derivatives have attracted great interest because of the molecular stability for device fabrication. Due to the strong $\pi-\pi$ stacking enhanced by steric hindrances of large TIPS groups, most of the TIPS-P derivatives exhibit excellent crystallinity and some possess similar crystal structures, making them appropriate for constructing a homogeneous blending model. Considering the "exotic" bandlike transport behavior of localized charges in TIPS-P has been successfully explained by the quantum nuclear tunneling model, we take two TIPS-P derivatives, 8F-TIPS-P and 4Cl-TIPS-P (Figure 5a), to investigate the blending effect by using the quantum nuclear tunneling model and give thorough insight into the relationship between blending ratio and mobility.

DOI: 10.1021/acs.jctc.8b00779
J. Chem. Theory Comput. 2019, 15, 1477−1491

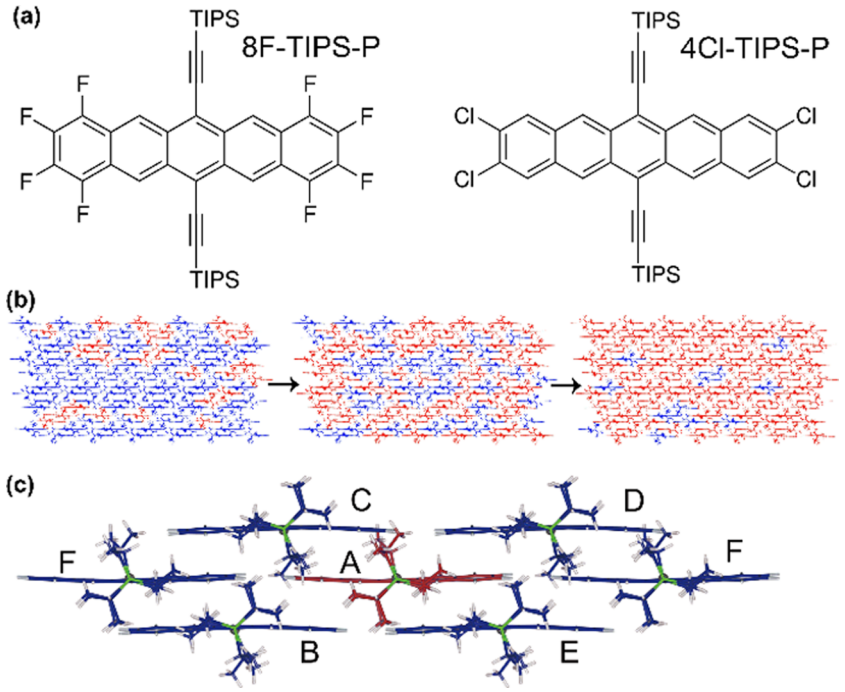

Figure 5. (a) Molecular structures of 8F-TIPS-P and 4Cl-TIPS-P. (b) Schematic representations of the random 4Cl-TIPS-P (red) substitution in 8F-TIPS-P (blue) crystal structure. The substitution ratio is 0.2, 0.5, and 0.8, respectively. (c) All possible charge transfer pathways from the red molecule (8F-TIPS-P or 4Cl-TIPS-P) to six neighbor blue molecules (8F-TIPS-P or 4Cl-TIPS-P). Figure adapted with permission from Society of Photo-Optical Instrumentation Engineers (ref 92).

Among moderately substituted TIPS-P derivatives, 8F-TIPS-P and 4Cl-TIPS-P have relatively compatible energy levels as well as similar molecular structures. Thus, in the blending model, the two molecules are blended homogeneously based on the reported crystal structure of 8F-TIPS-P. The ratio of 4Cl-TIPS-P increases from 0 to 1 by randomly replacing the 8F-TIPS-P molecule with 4Cl-TIPS-P, as shown in Figure 5b. Since 8F-TIPS-P is n-type material and an isomer of 4Cl-TIPS-P is ambipolar material,[93] the calculations have been focused on electron transport in the 2D network.

Huang–Rhys factors and charge reorganization energies for normal modes have been calculated and along with the intermolecular transfer integrals are depicted in Figure 5c and Table 7. The total reorganization energies of 8F-TIPS-P and 4Cl-TIPS-P are equal to 252 and 188 meV, respectively. The site energy difference of the electron transfer process from 8F-TIPS-P to 4Cl-TIPS-P is 48.1 meV obtained from the orbital energies of optimized structures based on Koopmans' theorem. It should be noted that there are a total of 20 different pairs of charge hopping pathways which may happen in the blending systems (Figure 5c). Therefore, by using this site energy difference value, 20 CT rates have been calculated by eq 1, and the temperature dependence of four selected CT rates ($k_{A\rightarrow E}$) from 50 to 300 K have been plotted in Figure 6. From 8F-TIPS-P to 8F-TIPS-P or 4Cl-TIPS-P, the CT rate increases with temperature, indicating a thermal-activated process; but it is observed that the CT rate to 4Cl-TIPS-P vanishes dramatically upon cooling, due to the higher site energy at the acceptor. The CT rate from 4Cl-TIPS-P to 4Cl-TIPS-P or 8F-TIPS-P is decreasing with rising temperature, which should be attributed to the strong quantum nuclear tunneling effect.

Table 7. Transfer Integrals (meV) between 8F-TIPS-P (8F) and 4Cl-TIPS-P (4Cl)[a]

	type of the start and end molecules			
pathway	8F → 8F	8F → 4Cl	4Cl → 8F	4Cl → 4Cl
A → B	19.3	30.1	30.2	40.0
A → C	0.7	8.1	8.0	15.6
A → D	0.4	6.8	6.8	10.5
A → E	130.2	150.9	150.9	170.3
A → F	0.4	4.5	4.5	25.3

[a]Table adapted with permission from Society of Photo-Optical Instrumentation Engineers (ref 92).

Based on the CT rates, the relations between electron mobility and blending ratio (r) under different temperatures have been investigated, see Figure 7a. For pure 8F-TIPS-P (r = 1), the mobility is almost independent of temperature, while for pure 4Cl-TIPS-P (r = 0), the mobility decreases with temperature. Marcus mobilities for pure 8F-TIPS-P and 4Cl-TIPS-P at 300 K are 0.32 and 2.7 $cm^2\ V^{-1}\ s^{-1}$ separately, while quantum mobilities are 0.40 and 7.6 $cm^2\ V^{-1}\ s^{-1}$, indicating 4Cl-TIPS-P possesses a much stronger nuclear tunneling effect than 8F-TIPS-P. Then, in order to further understand the blending effect on mobility, the relations between blending ratio and mobility at 50 and 300 K have been presented in Figure 7b. It shows that when T = 300 K, the mobility increases smoothly as the ratio of 4Cl-TIPS-P increases. However, in the case of T = 50 K, the mobility is reduced as the ratio of 4Cl-TIPS-P until only 5% 8F-TIPS-P is left, see Figures 7b and 7c. After that point, the mobility is sharply increased to a global maximum, namely the mobility for pure 4Cl-TIPS-P. A similar trend has been observed experimentally in the zinc phthalocyanine system,[86] demonstrating the rationalization of our study. Mixing 0.1% of 8F-TIPS-P in 4Cl-TIPS-P would reduce the mobility by 2 orders of magnitude when T = 50 K. Such a significant impact on

DOI: 10.1021/acs.jctc.8b00779
J. Chem. Theory Comput. 2019, 15, 1477–1491

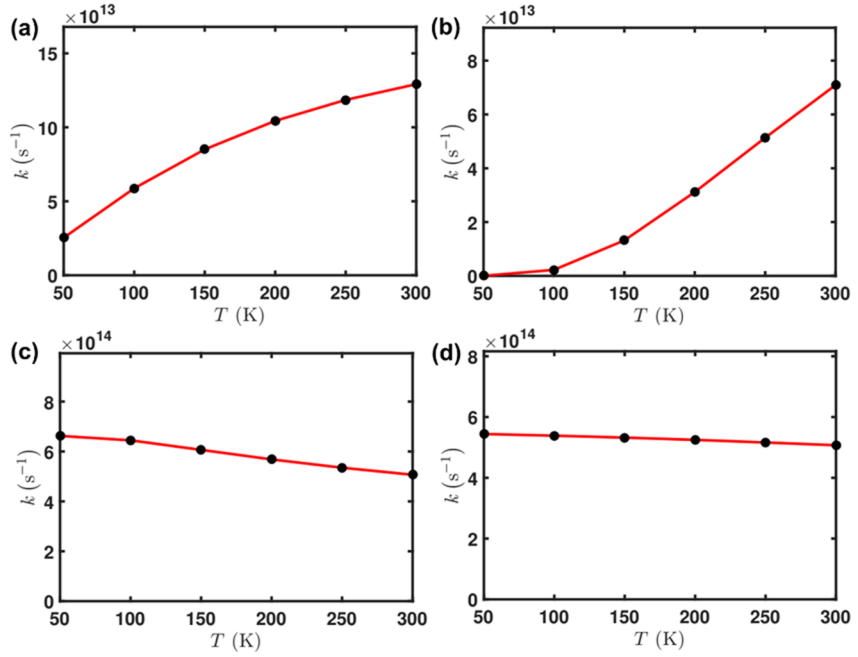

Figure 6. Temperature dependence of the charge transfer rate between 8F-TIPS-P and 4Cl-TIPS-P: (a) from 8F-TIPS-P to 8F-TIPS-P, (b) from 8F-TIPS-P to 4Cl-TIPS-P, (c) from 4Cl-TIPS-P to 8F-TIPS-P, and (d) from 4Cl-TIPS-P to 4Cl-TIPS-P. Figure adapted with permission from Society of Photo-Optical Instrumentation Engineers (ref 92).

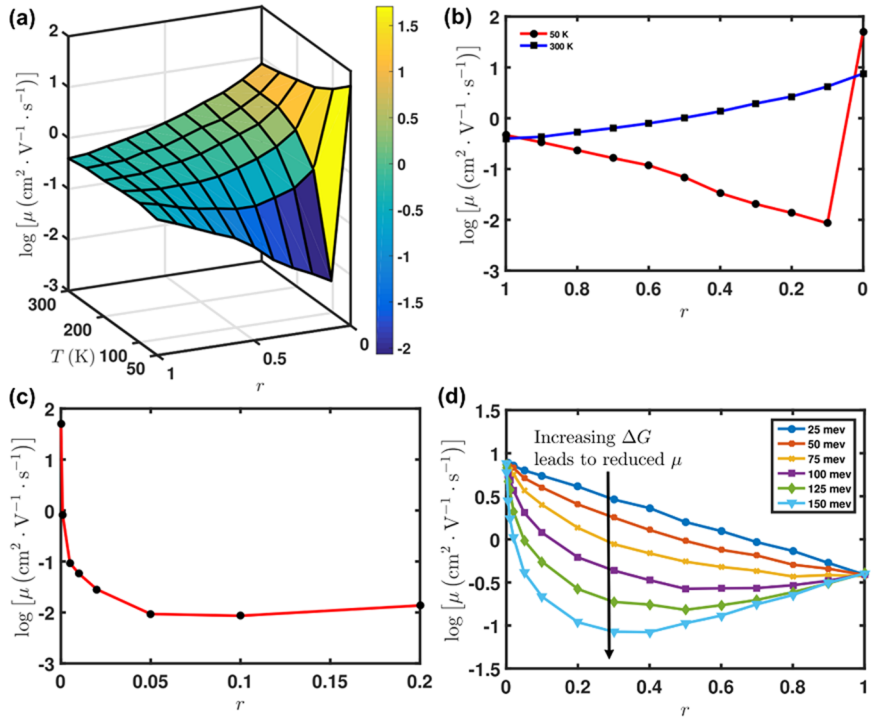

Figure 7. (a) Ratio of 8F-TIPS-P (r) and temperature (T) dependence of the mobility (μ) of 8F-TIPS-P and 4Cl-TIPS-P blending system. (b) $\mu(r)$ when T = 50 and 300 K, respectively. (c) Ratio of 8F-TIPS-P dependence of μ when T = 50 K. (d) Dependence of μ on r when ΔG = 25, 50, 75, 100, 125, and 150 meV, respectively, at T = 300 K. Figure adapted with permission from Society of Photo-Optical Instrumentation Engineers (ref 92).

mobility by minor 8F-TIPS-P doping can be ascribed to the fact that the LUMO of 8F-TIPS-P lies between the HOMO and LUMO of 4Cl-TIPS-P thus becoming the trap for electrons. Since the electron transfer from 8F-TIPS-P to 4Cl-TIPS-P is energetically unfavored, it is extremely difficult at low temperature. In fact, the CT rate from 8F-TIPS-P to 4Cl-TIPS-P at 50 K is only 0.01% of that at 300 K, as shown in Figure 7b. Hence, such a mechanism provides an explanation for the experimentally observed nonmonotonic temperature dependence of mobility, where mobility first increases and then decreases upon rising temperature.[10,75,94,95] At relatively low temperature, transport is limited by traps induced by

DOI: 10.1021/acs.jctc.8b00779
J. Chem. Theory Comput. 2019, 15, 1477−1491

impurities, and increasing temperature results in higher mobility; whereas at higher temperature range, the nuclear tunneling effect becomes dominated in charge transport, so that increasing temperature would hinder charge mobility.

At last, the effect of site energy difference (ΔG) on mobility for blending systems has been tested with T fixed at 300 K. The result shown in Figure 7d demonstrates that blending tends to reduce charge mobility with enhanced ΔG. Since the trap depth is positive related to ΔG, with larger ΔG, the CT rates between energetically favored and unfavored pathways vary dramatically, and then charge carriers fall into the deeper traps to avoid escaping. Nevertheless, when ΔG is small (<50 meV), the trapping effect is negligible, so the charge transport in a blending system would behave as a simple mixture.

5. CONCLUSIONS AND OUTLOOK

In summary, we have presented systematic investigations on the microscopic mechanisms in charge transport for organic semiconductors by adopting different methods covered from the semiclassical hopping, to quantum nuclear tunneling hopping, to quantum wavepacket diffusion, and finally to the bandlike model. First, we propose a feasible strategy to determine the transport mechanism on organic semiconductors by predicting the isotope effect in both hopping and bandlike pictures. No isotope effect could be observed if the semiclassical hopping model or acoustic phonon dominated bandlike model is dominated in charge transport. Only if the quantum nuclear tunneling effect exists can the isotope effect be found. Thus, in other words, when a noticeable isotope effect is observed by isotopic substitution on the positions involved actively in vibrations with large charge reorganization, the quantum nuclear tunneling should be certified. Furthermore, we apply four theories from hopping to bandlike on exploring the intrinsic charge transport property in a series of high mobility organic semiconductors. With such a comprehensive computational tool, the roles of quantum nuclear tunneling and charge delocalization effects on charge transport have been identified. It is demonstrated that the semiclassical Marcus theory always underestimates the mobility by ignoring the quantum nuclear effect, while the bandlike deformation potential theory overvalues the mobility due to the absence of the charge localization effect. Only quantum nuclear tunneling and TDWPD methods can provide reasonable prediction on high mobility for organics, demonstrating the universality of the quantum nuclear tunneling assisted polaron transport model for organic materials including conducting polymers. As for the systems with relatively strong delocalization effects, such as pentacene, DNTT, DATT, and PDIF-CN_2, a wavepacket description including the nuclear tunneling effect should be favored.

As with what has been introduced in section 3, we mainly focus on studying the intrinsic charge transport property in perfect crystalline OSCs. Nonetheless, organic materials for electronic devices generally exist in the form of amorphous films or defective crystals. Thus, besides the inherent microscopic mechanisms discussed above, some other microscopic factors also play important roles on influencing the transport dynamics, such as disorders/defects. In modeling charge transport, extended and correlated Gaussian disorder models[96−101] have achieved great successes in rationalizing the effect of finite carrier concentration, the spatial correlations of site energy, the shape of density of states, and positional disorders but not in terms of molecular descriptions. Thus, Kordt et al.,[102] Baumeier et al.,[103] Rühle et al.,[104] and Massé et al.[105] have developed stochastic models which generalize Gaussian disorder models to realistic amorphous OSCs by combining *ab initio* microscopic simulations of the morphology, charge transfer rate, and site energies. By employing the stochastic models, the dependences of the material morphology and molecular structure on carrier mobility can be obtained.[105−108] However, the CT rate formula used in them is the Marcus theory. The absence of the quantum nuclear effect makes these models lack predictability. Hence, to give a better prediction on charge transport behavior in OSCs, we can incorporate the quantum CT rate into the stochastic model in the future which will retain the influences of both quantum nuclear tunneling and site energy disorder.

AUTHOR INFORMATION

Corresponding Author

*E-mail: zgshuai@tisnghua.edu.cn.

ORCID

Yuqian Jiang: 0000-0002-7013-4704

Zhigang Shuai: 0000-0003-3867-2331

Funding

This work is supported by National Natural Science Foundation of China (Grant Nos. 21788102 and 21603043) and the Ministry of Science and Technology (Grant No. 2017YFA0204501).

Notes

The authors declare no competing financial interest.

ACKNOWLEDGMENTS

This virtual special issue to commemorate the 40th anniversary of the resumption of Gao Kao (Entrance Exam for Higher Education) has special meaning to Z.S., who participated in the very first one in the winter of 1977 as an in-school student, for the purpose of testing this exercise. Gao Kao is now the emblem of the resurrection of China while recovering from the calamitous cultural revolution. The following collaborators have made important contributions to the original work: Prof. Hua Geng, Prof. Yi Zhao, and Dr. Xinxin Zhong. Numerical calculations have been performed at the Tsinghua University high performance computation center.

REFERENCES

(1) Ebata, H.; Izawa, T.; Miyazaki, E.; Takimiya, K.; Ikeda, M.; Kuwabara, H.; Yui, T. Highly soluble [1] benzothieno [3, 2-b] benzothiophene (BTBT) derivatives for high-performance, solution-processed organic field-effect transistors. *J. Am. Chem. Soc.* **2007**, *129*, 15732−15733.

(2) Takimiya, K.; Shinamura, S.; Osaka, I.; Miyazaki, E. Thienoacene-Based Organic Semiconductors. *Adv. Mater.* **2011**, *23*, 4347−4370.

(3) Niimi, K.; Shinamura, S.; Osaka, I.; Miyazaki, E.; Takimiya, K. Dianthra [2, 3-b: 2′, 3′-f] thieno [3, 2-b] thiophene (DATT): Synthesis, Characterization, and FET Characteristics of New π-extended heteroarene with eight fused aromatic rings. *J. Am. Chem. Soc.* **2011**, *133*, 8732−8739.

(4) Kang, M. J.; Doi, I.; Mori, H.; Miyazaki, E.; Takimiya, K.; Ikeda, M.; Kuwabara, H. Alkylated Dinaphtho[2,3-b:2′,3′-f]Thieno[3,2-b]Thiophenes (Cn-DNTTs): Organic Semiconductors for High-Performance Thin-Film Transistors. *Adv. Mater.* **2011**, *23*, 1222−1225.

(5) Xie, W.; Willa, K.; Wu, Y.; Häusermann, R.; Takimiya, K.; Batlogg, B.; Frisbie, C. D. Temperature-Independent Transport in

DOI: 10.1021/acs.jctc.8b00779
J. Chem. Theory Comput. 2019, 15, 1477−1491

High-Mobility Dinaphtho-Thieno-Thiophene (DNTT) Single Crystal Transistors. *Adv. Mater.* **2013**, *25*, 3478−3484.
(6) Jurchescu, O. D.; Popinciuc, M.; van Wees, B. J.; Palstra, T. T. M. Interface-Controlled, High-Mobility Organic Transistors. *Adv. Mater.* **2007**, *19*, 688−692.
(7) Podzorov, V.; Menard, E.; Borissov, A.; Kiryukhin, V.; Rogers, J. A.; Gershenson, M. E. Intrinsic charge transport on the surface of organic semiconductors. *Phys. Rev. Lett.* **2004**, *93*, 086602−4.
(8) Zeis, R.; Besnard, C.; Siegrist, T.; Schlockermann, C.; Chi, X.; Kloc, C. Field Effect Studies on Rubrene and Impurities of Rubrene. *Chem. Mater.* **2006**, *18*, 244−248.
(9) Xie, W.; McGarry, K. A.; Liu, F.; Wu, Y.; Ruden, P. P.; Douglas, C. J.; Frisbie, C. D. High-Mobility Transistors Based on Single Crystals of Isotopically Substituted Rubrene-d28. *J. Phys. Chem. C* **2013**, *117*, 11522−11529.
(10) Sakanoue, T.; Sirringhaus, H. Band-like temperature dependence of mobility in a solution-processed organic semiconductor. *Nat. Mater.* **2010**, *9*, 736−740.
(11) Xi, J.; Long, M.; Tang, L.; Wang, D.; Shuai, Z. First-principles prediction of charge mobility in carbon and organic nanomaterials. *Nanoscale* **2012**, *4*, 4348−4369.
(12) Kobayashi, H.; Kobayashi, N.; Hosoi, S.; Koshitani, N.; Murakami, D.; Shirasawa, R.; Kudo, Y.; Hobara, D.; Tokita, Y.; Itabashi, M. Hopping and band mobilities of pentacene, rubrene, and 2, 7-dioctyl [1] benzothieno [3, 2-b][1] benzothiophene (C8-BTBT) from first principle calculations. *J. Chem. Phys.* **2013**, *139*, 014707−8.
(13) Brédas, J. L.; Calbert, J. P.; da Silva Filho, D. A.; Cornil, J. Organic semiconductors: A theoretical characterization of the basic parameters governing charge transport. *Proc. Natl. Acad. Sci. U. S. A.* **2002**, *99*, 5804−5809.
(14) Cornil, J.; Beljonne, D.; Calbert, J. P.; Brédas, J. L. Interchain Interactions in Organic π-Conjugated Materials: Impact on Electronic Structure, Optical Response, and Charge Transport. *Adv. Mater.* **2001**, *13*, 1053−1067.
(15) Coropceanu, V.; Cornil, J.; da Silva Filho, D. A.; Olivier, Y.; Silbey, R.; Brédas, J.-L. Charge Transport in Organic Semiconductors. *Chem. Rev.* **2007**, *107*, 926−952.
(16) Sokolov, A. N.; Atahan-Evrenk, S.; Mondal, R.; Akkerman, H. B.; Sánchez-Carrera, R. S.; Granados-Focil, S.; Schrier, J.; Mannsfeld, S. C.; Zoombelt, A. P.; Bao, Z. From computational discovery to experimental characterization of a high hole mobility organic crystal. *Nat. Commun.* **2011**, *2*, 437.
(17) Wang, L.; Nan, G.; Yang, X.; Peng, Q.; Li, Q.; Shuai, Z. Computational methods for design of organic materials with high charge mobility. *Chem. Soc. Rev.* **2010**, *39*, 423−434.
(18) Marcus, R. A. On the Theory of Oxidation-Reduction Reactions Involving Electron Transfer. I. *J. Chem. Phys.* **1956**, *24*, 966−978.
(19) Yuen, J. D.; Menon, R.; Coates, N. E.; Namdas, E. B.; Cho, S.; Hannahs, S. T.; Moses, D.; Heeger, A. J. Nonlinear transport in semiconducting polymers at high carrier densities. *Nat. Mater.* **2009**, *8*, 572−575.
(20) Dhoot, A.; Wang, G.; Moses, D.; Heeger, A. Voltage-induced metal-insulator transition in polythiophene field-effect transistors. *Phys. Rev. Lett.* **2006**, *96*, 246403−4.
(21) Asadi, K.; Kronemeijer, A. J.; Cramer, T.; Jan Anton Koster, L.; Blom, P. W. M.; de Leeuw, D. M. Polaron hopping mediated by nuclear tunnelling in semiconducting polymers at high carrier density. *Nat. Commun.* **2013**, *4*, 1710.
(22) Deng, W.-Q.; Goddard, W. A. Predictions of Hole Mobilities in Oligoacene Organic Semiconductors from Quantum Mechanical Calculations. *J. Phys. Chem. B* **2004**, *108*, 8614−8621.
(23) Ostroverkhova, O.; Cooke, D. G.; Shcherbyna, S.; Egerton, R. F.; Hegmann, F. A.; Tykwinski, R. R.; Anthony, J. E. Bandlike transport in pentacene and functionalized pentacene thin films revealed by subpicosecond transient photoconductivity measurements. *Phys. Rev. B: Condens. Matter Mater. Phys.* **2005**, *71*, 035204−6.
(24) Kronemeijer, A. J.; Huisman, E. H.; Katsouras, I.; van Hal, P. A.; Geuns, T. C. T.; Blom, P. W. M.; van der Molen, S. J.; de Leeuw, D. M. Universal Scaling in Highly Doped Conducting Polymer Films. *Phys. Rev. Lett.* **2010**, *105*, 156604−4.
(25) Rodin, A. S.; Fogler, M. M. Apparent Power-Law Behavior of Conductance in Disordered Quasi-One-Dimensional Systems. *Phys. Rev. Lett.* **2010**, *105*, 106801−4.
(26) Gorham-Bergeron, E.; Emin, D. Phonon-assisted hopping due to interaction with both acoustical and optical phonons. *Phys. Rev. B* **1977**, *15*, 3667−3680.
(27) Ulstrup, J.; Jortner, J. The effect of intramolecular quantum modes on free energy relationships for electron transfer reactions. *J. Chem. Phys.* **1975**, *63*, 4358−4368.
(28) Nan, G.; Yang, X.; Wang, L.; Shuai, Z.; Zhao, Y. Nuclear tunneling effects of charge transport in rubrene, tetracene, and pentacene. *Phys. Rev. B: Condens. Matter Mater. Phys.* **2009**, *79*, 115203−9.
(29) Geng, H.; Peng, Q.; Wang, L.; Li, H.; Liao, Y.; Ma, Z.; Shuai, Z. Toward Quantitative Prediction of Charge Mobility in Organic Semiconductors: Tunneling Enabled Hopping Model. *Adv. Mater.* **2012**, *24*, 3568−3572.
(30) Taherinia, D.; Smith, C. E.; Ghosh, S.; Odoh, S. O.; Balhorn, L.; Gagliardi, L.; Cramer, C. J.; Frisbie, C. D. Charge Transport in 4 nm Molecular Wires with Interrupted Conjugation: Combined Experimental and Computational Evidence for Thermally Assisted Polaron Tunneling. *ACS Nano* **2016**, *10*, 4372−4383.
(31) van der Kaap, N. J.; Katsouras, I.; Asadi, K.; Blom, P. W. M.; Koster, L. J. A.; de Leeuw, D. M. Charge transport in disordered semiconducting polymers driven by nuclear tunneling. *Phys. Rev. B: Condens. Matter Mater. Phys.* **2016**, *93*, 140206−5.
(32) Munn, R. W.; Siebrand, W. Theory of Charge Carrier Transport in Aromatic Hydrocarbon Crystals. *J. Chem. Phys.* **1970**, *52*, 6391−6406.
(33) Munn, R. W.; Nicholson, J. R.; Siebrand, W.; Williams, D. F. Evidence for an Isotope Effect on Electron Drift Mobilities in Anthracene Crystals. *J. Chem. Phys.* **1970**, *52*, 6442−6443.
(34) Morel, D. L.; Hermann, A. M. Isotope effect for electron mobility in anthracene. *Phys. Lett. A* **1971**, *36*, 101−102.
(35) Mey, W.; Sonnonstine, T. J.; Morel, D. L.; Hermann, A. M. Drift mobility of holes and electrons in perdeuterated anthracene single crystals. *J. Chem. Phys.* **1973**, *58*, 2542−2546.
(36) Schein, L. B.; McGhie, A. R. Band-hopping mobility transition in naphthalene and deuterated naphthalene. *Phys. Rev. B: Condens. Matter Mater. Phys.* **1979**, *20*, 1631−1639.
(37) Lin, S. H.; Bersohn, R. Effect of Partial Deuteration and Temperature on Triplet-State Lifetimes. *J. Chem. Phys.* **1968**, *48*, 2732−2736.
(38) Saltiel, J.; Waller, A. S.; Sears, D. F.; Garrett, C. Z. Fluorescence quantum yields of trans-stilbene-d(0) and trans-stilbene-d(2) in n-hexane and n-tetradecane - medium and deuterium-isotope effects on decay processes. *J. Phys. Chem.* **1993**, *97*, 2516−2522.
(39) Hewitt, J. T.; Concepcion, J. J.; Damrauer, N. H. Inverse Kinetic Isotope Effect in the Excited-State Relaxation of a Ru(II)−Aquo Complex: Revealing the Impact of Hydrogen-Bond Dynamics on Nonradiative Decay. *J. Am. Chem. Soc.* **2013**, *135*, 12500−12503.
(40) Bigeleisen, J.; Wolfsberg, M. Theoretical and experimental aspects of isotope effects in chemical kinetics. *Adv. Chem. Phys.* **1958**, *1*, 15−76.
(41) Ludlow, M. K.; Soudackov, A. V.; Hammes-Schiffer, S. Theoretical analysis of the unusual temperature dependence of the kinetic isotope effect in quinol oxidation. *J. Am. Chem. Soc.* **2009**, *131*, 7094−7102.
(42) Hazra, A.; Soudackov, A. V.; Hammes-Schiffer, S. Isotope Effects on the Nonequilibrium Dynamics of Ultrafast Photoinduced Proton-Coupled Electron Transfer Reactions in Solution. *J. Phys. Chem. Lett.* **2011**, *2*, 36−40.
(43) Wang, L.; Beljonne, D. Flexible Surface Hopping Approach to Model the Crossover from Hopping to Band-like Transport in Organic Crystals. *J. Phys. Chem. Lett.* **2013**, *4*, 1888−1894.

DOI: 10.1021/acs.jctc.8b00779
J. Chem. Theory Comput. 2019, 15, 1477−1491

(44) Troisi, A.; Orlandi, G. Charge-transport regime of crystalline organic semiconductors: diffusion limited by thermal off-diagonal electronic disorder. *Phys. Rev. Lett.* **2006**, *96*, 086601−4.
(45) Gao, X.; Geng, H.; Peng, Q.; Ren, J.; Yi, Y.; Wang, D.; Shuai, Z. Nonadiabatic Molecular Dynamics Modeling of the Intrachain Charge Transport in Conjugated Diketopyrrolo-pyrrole Polymers. *J. Phys. Chem. C* **2014**, *118*, 6631−6640.
(46) Zhang, X.; Li, Z.; Lu, G. First-principles simulations of exciton diffusion in organic semiconductors. *Phys. Rev. B: Condens. Matter Mater. Phys.* **2011**, *84*, 235208−8.
(47) Wang, D.; Chen, L.; Zheng, R.; Wang, L.; Shi, Q. Communications: A nonperturbative quantum master equation approach to charge carrier transport in organic molecular crystals. *J. Chem. Phys.* **2010**, *132*, 081101−4.
(48) Zhong, X.; Zhao, Y. Non-Markovian stochastic Schrödinger equation at finite temperatures for charge carrier dynamics in organic crystals. *J. Chem. Phys.* **2013**, *138*, 014111−9.
(49) Zhong, X.; Zhao, Y. Charge carrier dynamics in phonon-induced fluctuation systems from time-dependent wavepacket diffusion approach. *J. Chem. Phys.* **2011**, *135*, 134110−9.
(50) Zhang, W.; Zhong, X.; Zhao, Y. Electron Mobilities of n-Type Organic Semiconductors from Time-Dependent Wavepacket Diffusion Method: Pentacenequinone Derivatives. *J. Phys. Chem. A* **2012**, *116*, 11075−11082.
(51) Shuai, Z.; Geng, H.; Xu, W.; Liao, Y.; Andre, J.-M. From charge transport parameters to charge mobility in organic semiconductors through multiscale simulation. *Chem. Soc. Rev.* **2014**, *43*, 2662−2679.
(52) Xi, J.; Wang, D.; Yi, Y.; Shuai, Z. Electron-phonon couplings and carrier mobility in graphynes sheet calculated using the Wannier-interpolation approach. *J. Chem. Phys.* **2014**, *141*, 034704−10.
(53) Tang, L.; Long, M.; Wang, D.; Shuai, Z. The role of acoustic phonon scattering in charge transport in organic semiconductors: a first-principles deformation-potential study. *Sci. China, Ser. B: Chem.* **2009**, *52*, 1646−1652.
(54) Shi, W.; Chen, J.; Xi, J.; Wang, D.; Shuai, Z. Search for Organic Thermoelectric Materials with High Mobility: The Case of 2,7-Dialkyl[1]benzothieno[3,2-b][1]benzothiophene Derivatives. *Chem. Mater.* **2014**, *26*, 2669−2677.
(55) Shi, W.; Zhao, T.; Xi, J.; Wang, D.; Shuai, Z. Unravelling Doping Effects on PEDOT at the Molecular Level: From Geometry to Thermoelectric Transport Properties. *J. Am. Chem. Soc.* **2015**, *137*, 12929−12938.
(56) Kresse, G.; Furthmüller, J. Efficient iterative schemes for *ab initio* total-energy calculations using a plane-wave basis set. *Phys. Rev. B: Condens. Matter Mater. Phys.* **1996**, *54*, 11169−11186.
(57) Scheidemantel, T. J.; Ambrosch-Draxl, C.; Thonhauser, T.; Badding, J. V.; Sofo, J. O. Transport coefficients from first-principles calculations. *Phys. Rev. B: Condens. Matter Mater. Phys.* **2003**, *68*, 125210−6.
(58) Yang, J.; Li, H.; Wu, T.; Zhang, W.; Chen, L.; Yang, J. Evaluation of Half-Heusler Compounds as Thermoelectric Materials Based on the Calculated Electrical Transport Properties. *Adv. Funct. Mater.* **2008**, *18*, 2880−2888.
(59) Tsutsui, Y.; Schweicher, G.; Chattopadhyay, B.; Sakurai, T.; Arlin, J. B.; Ruzié, C.; Aliev, A.; Ciesielski, A.; Colella, S.; Kennedy, A. R.; Lemaur, V.; Olivier, Y.; Hadji, R.; Sanguinet, L.; Castet, F.; Osella, S.; Dudenko, D.; Beljonne, D.; Cornil, J.; Samorì, P.; Seki, S.; Geerts, Y. H. Unraveling unprecedented charge carrier mobility through structure property relationship of four isomers of didodecyl[1]-benzothieno[3,2-b][1]benzothiophene. *Adv. Mater.* **2016**, *28*, 7106−7114.
(60) Young, W. M.; Elcock, E. W. Monte Carlo studies of vacancy migration in binary ordered alloys: I. *Proc. Phys. Soc., London* **1966**, *89*, 735−746.
(61) Zhan, X. W.; Facchetti, A.; Barlow, S.; Marks, T. J.; Ratner, M. A.; Wasielewski, M. R.; Marder, S. R. Rylene and Related Diimides for Organic Electronics. *Adv. Mater.* **2011**, *23*, 268−284.
(62) Shukla, D.; Nelson, S. F.; Freeman, D. C.; Rajeswaran, M.; Ahearn, W. G.; Meyer, D. M.; Carey, J. T. Thin-Film Morphology Control in Naphthalene-Diimide-Based Semiconductors: High Mobility n-Type Semiconductor for Organic Thin-Film Transistors. *Chem. Mater.* **2008**, *20*, 7486−7491.
(63) Briseno, A. L.; Mannsfeld, S. C. B.; Reese, C.; Hancock, J. M.; Xiong, Y.; Jenekhe, S. A.; Bao, Z.; Xia, Y. Perylenediimide Nanowires and Their Use in Fabricating Field-Effect Transistors and Complementary Inverters. *Nano Lett.* **2007**, *7*, 2847−2853.
(64) Chesterfield, R. J.; McKeen, J. C.; Newman, C. R.; Ewbank, P. C.; da Silva Filho, D. A.; Brédas, J.-L.; Miller, L. L.; Mann, K. R.; Frisbie, C. D. Organic Thin Film Transistors Based on N-Alkyl Perylene Diimides: Charge Transport Kinetics as a Function of Gate Voltage and Temperature. *J. Phys. Chem. B* **2004**, *108*, 19281−19292.
(65) Becke, A. D. Density-functional thermochemistry. III. The role of exact exchange. *J. Chem. Phys.* **1993**, *98*, 5648−5652.
(66) Lee, C.; Yang, W.; Parr, R. G. Development of the Colle-Salvetti correlation-energy formula into a functional of the electron density. *Phys. Rev. B: Condens. Matter Mater. Phys.* **1988**, *37*, 785−789.
(67) Frisch, M. J.; Trucks, G. W.; Schlegel, H. B.; Scuseria, G. E.; Robb, M. A.; Cheeseman, J. R.; Scalmani, G.; Barone, V.; Mennucci, B.; Petersson, G. A.; Nakatsuji, H.; Caricato, M.; Li, X.; Hratchian, H. P.; Izmaylov, A. F.; Bloino, J.; Zheng, G.; Sonnenberg, J. L.; Hada, M.; Ehara, M.; Toyota, K.; Fukuda, R.; Hasegawa, J.; Ishida, M.; Nakajima, T.; Honda, Y.; Kitao, O.; Nakai, H.; Vreven, T.; Montgomery, J. A., Jr.; Peralta, J. E.; Ogliaro, F.; Bearpark, M.; Heyd, J. J.; Brothers, E.; Kudin, K. N.; Staroverov, V. N.; Kobayashi, R.; Normand, J.; Raghavachari, K.; Rendell, A.; Burant, J. C.; Iyengar, S. S.; Tomasi, J.; Cossi, M.; Rega, N.; Millam, M. J.; Klene, M.; Knox, J. E.; Cross, J. B.; Bakken, V.; Adamo, C.; Jaramillo, J.; Gomperts, R.; Stratmann, R. E.; Yazyev, O.; Austin, A. J.; Cammi, R.; Pomelli, C.; Ochterski, J. W.; Martin, R. L.; Morokuma, K.; Zakrzewski, V. G.; Voth, G. A.; Salvador, P.; Dannenberg, J. J.; Dapprich, S.; Daniels, A. D.; Farkas, Ö.; Foresman, J. B.; Ortiz, J. V.; Cioslowski, J.; Fox, D. J. *Gaussian 09*, Revision D.01; Gaussian Inc.: Wallingford, CT, 2009.
(68) Reimers, J. R. A practical method for the use of curvilinear coordinates in calculations of normal-mode-projected displacements and Duschinsky rotation matrices for large molecules. *J. Chem. Phys.* **2001**, *115*, 9103−9109.
(69) Jurchescu, O. D.; Meetsma, A.; Palstra, T. T. Low-temperature structure of rubrene single crystals grown by vapor transport. *Acta Crystallogr., Sect. B: Struct. Sci.* **2006**, *62*, 330−334.
(70) Perdew, J. P.; Chevary, J. A.; Vosko, S. H.; Jackson, K. A.; Pederson, M. R.; Singh, D. J.; Fiolhais, C. Atoms, molecules, solids, and surfaces: Applications of the generalized gradient approximation for exchange and correlation. *Phys. Rev. B: Condens. Matter Mater. Phys.* **1992**, *46*, 6671−6687.
(71) Valeev, E. F.; Coropceanu, V.; da Silva Filho, D. A.; Salman, S.; Brédas, J.-L. Effect of Electronic Polarization on Charge-Transport Parameters in Molecular Organic Semiconductors. *J. Am. Chem. Soc.* **2006**, *128*, 9882−9886.
(72) Niu, Y.; Li, W.; Peng, Q.; Geng, H.; Yi, Y.; Wang, L.; Nan, G.; Wang, D.; Shuai, Z. MOlecular MAterials Property Prediction Package (MOMAP) 1.0: a software package for predicting the luminescent properties and mobility of organic functional materials. *Mol. Phys.* **2018**, *116*, 1078−1090.
(73) Jiang, Y.; Geng, H.; Shi, W.; Peng, Q.; Zheng, X.; Shuai, Z. Theoretical Prediction of Isotope Effects on Charge Transport in Organic Semiconductors. *J. Phys. Chem. Lett.* **2014**, *5*, 2267−2273.
(74) He, T.; Stolte, M.; Würthner, F. Air-Stable n-Channel Organic Single Crystal Field-Effect Transistors Based on Microribbons of Core-Chlorinated Naphthalene Diimide. *Adv. Mater.* **2013**, *25*, 6951−6955.
(75) Minder, N. A.; Ono, S.; Chen, Z.; Facchetti, A.; Morpurgo, A. F. Band-Like Electron Transport in Organic Transistors and Implication of the Molecular Structure for Performance Optimization. *Adv. Mater.* **2012**, *24*, 503−508.
(76) Lee, B.; Chen, Y.; Fu, D.; Yi, H.; Czelen, K.; Najafov, H.; Podzorov, V. Trap healing and ultralow-noise Hall effect at the surface of organic semiconductors. *Nat. Mater.* **2013**, *12*, 1125−1129.

DOI: 10.1021/acs.jctc.8b00779
J. Chem. Theory Comput. 2019, 15, 1477−1491

(77) Jiang, Y.; Peng, Q.; Geng, H.; Ma, H.; Shuai, Z. Negative isotope effect for charge transport in acenes and derivatives - A theoretical conclusion. *Phys. Chem. Chem. Phys.* **2015**, *17*, 3273−3280.
(78) Newton, M. D.; Sutin, N. Electron Transfer Reactions in Condensed Phases. *Annu. Rev. Phys. Chem.* **1984**, *35*, 437−480.
(79) Talezer, H.; Kosloff, R. An accurate and efficient scheme for propagating the time-dependent schrodinger-equation. *J. Chem. Phys.* **1984**, *81*, 3967−3971.
(80) Wang, L.; Li, Q.; Shuai, Z.; Chen, L.; Shi, Q. Multiscale study of charge mobility of organic semiconductor with dynamic disorders. *Phys. Chem. Chem. Phys.* **2010**, *12*, 3309−3314.
(81) Nan, G.; Li, Z. Influence of lattice dynamics on charge transport in the dianthra [2, 3-b: 2′, 3′-f]-thieno [3, 2-b] thiophene organic crystals from a theoretical study. *Phys. Chem. Chem. Phys.* **2012**, *14*, 9451−9459.
(82) Sundar, V. C.; Zaumseil, J.; Podzorov, V.; Menard, E.; Willett, R. L.; Someya, T.; Gershenson, M. E.; Rogers, J. A. Elastomeric Transistor Stamps: Reversible Probing of Charge Transport in Organic Crystals. *Science* **2004**, *303*, 1644−1646.
(83) Ling, M.-M.; Reese, C.; Briseno, A. L.; Bao, Z. Non-destructive probing of the anisotropy of field-effect mobility in the rubrene single crystal. *Synth. Met.* **2007**, *157*, 257−260.
(84) Jiang, Y.; Zhong, X.; Shi, W.; Peng, Q.; Geng, H.; Zhao, Y.; Shuai, Z. Nuclear quantum tunnelling and carrier delocalization effects to bridge the gap between hopping and bandlike behaviors in organic semiconductors. *Nanoscale Horiz.* **2016**, *1*, 53−59.
(85) Molinari, A. S.; Alves, H.; Chen, Z.; Facchetti, A.; Morpurgo, A. F. High Electron Mobility in Vacuum and Ambient for PDIF-CN2 Single-Crystal Transistors. *J. Am. Chem. Soc.* **2009**, *131*, 2462−2463.
(86) Schwarze, M.; Tress, W.; Beyer, B.; Gao, F.; Scholz, R.; Poelking, C.; Ortstein, K.; Gunther, A. A.; Kasemann, D.; Andrienko, D.; Leo, K. Band structure engineering in organic semiconductors. *Science* **2016**, *352*, 1446−1449.
(87) Fong, H. H.; Lun, K. C.; So, S. K. Hole transports in molecularly doped triphenylamine derivative. *Chem. Phys. Lett.* **2002**, *353*, 407−413.
(88) Tsung, K. K.; So, S. K. Carrier trapping and scattering in amorphous organic hole transporter. *Appl. Phys. Lett.* **2008**, *92*, 103315−3.
(89) Li, C.; Duan, L.; Sun, Y.; Li, H.; Qiu, Y. Charge Transport in Mixed Organic Disorder Semiconductors: Trapping, Scattering, and Effective Energetic Disorder. *J. Phys. Chem. C* **2012**, *116*, 19748−19754.
(90) Li, C.; Duan, L.; Li, H.; Qiu, Y. Universal Trap Effect in Carrier Transport of Disordered Organic Semiconductors: Transition from Shallow Trapping to Deep Trapping. *J. Phys. Chem. C* **2014**, *118*, 10651−10660.
(91) Bässler, H. charge transport in disordered organic photo-conductors - A monte-carlo simulation study. *Phys. Status Solidi B* **1993**, *175*, 15−56.
(92) Li, W.; Shuai, Z.; Geng, H. Theoretical insights into molecular blending on charge transport properties in organic semiconductors based on quantum nuclear tunneling model. *J. Photonics Energy* **2018**, *8*, 032204.
(93) Fan, J.-X.; Chen, X.-K.; Zhang, S.-F.; Ren, A.-M. Theoretical Study on Charge Transport Properties of Intra- and Extra-Ring Substituted Pentacene Derivatives. *J. Phys. Chem. A* **2016**, *120*, 2390−2400.
(94) Krupskaya, Y.; Gibertini, M.; Marzari, N.; Morpurgo, A. F. Band-Like Electron Transport with Record-High Mobility in the TCNQ Family. *Adv. Mater.* **2015**, *27*, 2453−2458.
(95) Xu, X.; Yao, Y.; Shan, B.; Gu, X.; Liu, D.; Liu, J.; Xu, J.; Zhao, N.; Hu, W.; Miao, Q. Electron Mobility Exceeding 10 $cm^2 V^{-1} s^{-1}$ and Band-Like Charge Transport in Solution-Processed n-Channel Organic Thin-Film Transistors. *Adv. Mater.* **2016**, *28*, 5276−5283.
(96) Massé, A.; Coehoorn, R.; Bobbert, P. A. Universal Size-Dependent Conductance Fluctuations in Disordered Organic Semiconductors. *Phys. Rev. Lett.* **2014**, *113*, 116604−5.
(97) Bässler, H. Charge transport in disordered organic photoconductors a Monte Carlo simulation study. *Phys. Status Solidi B* **1993**, *175*, 15−56.
(98) Novikov, S. V.; Dunlap, D. H.; Kenkre, V. M.; Parris, P. E.; Vannikov, A. V. Essential Role of Correlations in Governing Charge Transport in Disordered Organic Materials. *Phys. Rev. Lett.* **1998**, *81*, 4472−4475.
(99) Walker, A. B.; Kambili, A.; Martin, S. J. Electrical transport modelling in organic electroluminescent devices. *J. Phys.: Condens. Matter* **2002**, *14*, 9825−9876.
(100) Pasveer, W. F.; Cottaar, J.; Tanase, C.; Coehoorn, R.; Bobbert, P. A.; Blom, P. W. M.; de Leeuw, D. M.; Michels, M. A. J. Unified Description of Charge-Carrier Mobilities in Disordered Semiconducting Polymers. *Phys. Rev. Lett.* **2005**, *94*, 206601−4.
(101) Papadopoulos, T. A.; Muccioli, L.; Athanasopoulos, S.; Walker, A. B.; Zannoni, C.; Beljonne, D. Does supramolecular ordering influence exciton transport in conjugated systems? Insight from atomistic simulations. *Chem. Sci.* **2011**, *2*, 1025−1032.
(102) Kordt, P.; Stenzel, O.; Baumeier, B.; Schmidt, V.; Andrienko, D. Parametrization of Extended Gaussian Disorder Models from Microscopic Charge Transport Simulations. *J. Chem. Theory Comput.* **2014**, *10*, 2508−2513.
(103) Baumeier, B.; Stenzel, O.; Poelking, C.; Andrienko, D.; Schmidt, V. Stochastic modeling of molecular charge transport networks. *Phys. Rev. B: Condens. Matter Mater. Phys.* **2012**, *86*, 184202−7.
(104) Rühle, V.; Lukyanov, A.; May, F.; Schrader, M.; Vehoff, T.; Kirkpatrick, J.; Baumeier, B.; Andrienko, D. Microscopic Simulations of Charge Transport in Disordered Organic Semiconductors. *J. Chem. Theory Comput.* **2011**, *7*, 3335−3345.
(105) Massé, A.; Friederich, P.; Symalla, F.; Liu, F.; Nitsche, R.; Coehoorn, R.; Wenzel, W.; Bobbert, P. A. Ab initio charge-carrier mobility model for amorphous molecular semiconductors. *Phys. Rev. B: Condens. Matter Mater. Phys.* **2016**, *93*, 195209−9.
(106) Kordt, P.; Stodtmann, S.; Badinski, A.; Al Helwi, M.; Lennartz, C.; Andrienko, D. Parameter-free continuous drift-diffusion models of amorphous organic semiconductors. *Phys. Chem. Chem. Phys.* **2015**, *17*, 22778−22783.
(107) Kordt, P.; Speck, T.; Andrienko, D. Finite-size scaling of charge carrier mobility in disordered organic semiconductors. *Phys. Rev. B: Condens. Matter Mater. Phys.* **2016**, *94*, 014208−6.
(108) Poelking, C.; Cho, E.; Malafeev, A.; Ivanov, V.; Kremer, K.; Risko, C.; Brédas, J.-L.; Andrienko, D. Characterization of Charge-Carrier Transport in Semicrystalline Polymers: Electronic Couplings, Site Energies, and Charge-Carrier Dynamics in Poly(bithiophene-alt-thienothiophene) [PBTTT]. *J. Phys. Chem. C* **2013**, *117*, 1633−1640.

DOI: 10.1021/acs.jctc.8b00779
J. Chem. Theory Comput. 2019, 15, 1477−1491